INVESTIGATING THE EFFECTS OF OUTBURSTS ON PULSARS, THE CASE OF 2S 1417-624

A THESIS SUBMITTED TO
THE GRADUATE SCHOOL OF NATURAL AND APPLIED SCIENCES
OF
MIDDLE EAST TECHNICAL UNIVERSITY

BY

ÖZGÜR CAN ÖZÜDOĞRU

IN PARTIAL FULFILLMENT OF THE REQUIREMENTS
FOR
THE DEGREE OF MASTER OF SCIENCE
IN
PHYSICS

JUNE 2022

Approval of the thesis:

INVESTIGATING THE EFFECTS OF OUTBURSTS ON PULSARS, THE CASE OF 2S 1417-624

submitted by **ÖZGÜR CAN ÖZÜDOĞRU** in partial fulfillment of the requirements for the degree of **Master of Science in Physics Department, Middle East Technical University** by,

Prof. Dr. Halil Kalıpçılar
Dean, Graduate School of **Natural and Applied Sciences** _____

Prof. Dr. Seçkin Kürkçüoğlu
Head of Department, **Physics** _____

Prof. Dr. Altan Baykal
Supervisor, **Physics, METU** _____

Assist. Prof. Dr. Muhammed Miraç Serim
Co-supervisor, **School of Engineering, Atılım University** _____

Examining Committee Members:

Prof. Dr. Sıtkı Çağdaş İnam
Electrical and Electronics Engineering, Başkent University _____

Prof. Dr. Altan Baykal
Physics, METU _____

Assist. Prof. Dr. Muhammed Miraç Serim
Faculty of Engineering, Atılım University _____

Assoc. Prof. Dr. Burak Yedierler
Physics, METU _____

Prof. Dr. Rikkat Civelek
Physics, METU _____

Date:

I hereby declare that all information in this document has been obtained and presented in accordance with academic rules and ethical conduct. I also declare that, as required by these rules and conduct, I have fully cited and referenced all material and results that are not original to this work.

Name, Surname: Özgür Can Özüdoğru

Signature :

ABSTRACT

INVESTIGATING THE EFFECTS OF OUTBURSTS ON PULSARS, THE CASE OF 2S 1417-624

Özüdoğru, Özgür Can
M.S., Department of Physics
Supervisor: Prof. Dr. Altan Baykal
Co-Supervisor: Assist. Prof. Dr. Muhammed Miraç Serim

June 2022, 54 pages

This thesis examines the relationship with physical properties of neutron stars and their disturbances due to an outburst, focusing on particular case of 2S 1417-624 which exhibited a giant outburst in 2018.The entire outburst duration is monitored with The Neutron Star Inner Composition Explorer, which carried out Target of Opportunity observations of 2S 1417-624 between April 1 and September 2018.

The extracted lightcurve of all the NICER observations demonstrates the flux evolution of the source during the outburst. Additionally in the case of periodogram analysis, the spin period of the source is measured to be around 17.4 s which is clearly consistent with the frequency signal in the power spectrum and high signal-to-noise ratio pulse profiles generated with epoch folding. While individual power spectra for each observation are investigated, one of them provides a marginal signal around 1 Hz which is interpreted as a possible quasi-periodic oscillation. Pulse profiles demonstrates variability with the change in luminosity due to the outburst. This implies that there is a luminosity dependent change in the accretion geometry. Therefore, this thesis aims to understand the variations of geometry in terms of spectral evolution,

using a partial covering absorber model to reveal the accretion geometry along the line of sight. Time resolved spectral parameter changes show a contribution of an external partial covering component hydrogen column density of which are found to be in similar evolution with the flux.

Photon index of the power law and covering fraction of the partial covering model provides very similar evolutionary structures and these relational configurations are mutually confined to change as the accretion regime transition takes place (i.e. from sub-critical to super critical and vice versa.) However, the evolution of the spectral parameters do not show any sign for transition from gas dominated disc to radiation dominated disc at supercritical regime below 12 keV. However, flux evolution of the spectral parameters show consistent results in photon index with previous outbursts and reveals physical information regarding the partially covering material and the transition in the accretion geometry due to the increasing flux values.

Keywords: neutron stars, X-ray binaries, accretion dics, 2S 1417-624

ÖZ

MADDE FIŞKIRMALARININ NÖTRON YILDIZLARINA ETKİLERİNİN ARAŞTIRMASI, 2S 1417-624 ÖRNEĞİ

Özüdoğru, Özgür Can
Yüksek Lisans, Fizik Bölümü
Tez Yöneticisi: Prof. Dr. Altan Baykal
Ortak Tez Yöneticisi: Dr. Öğr. Üyesi. Muhammed Miraç Serim

Haziran 2022 , 54 sayfa

Bu tezde, nötron yıldızlarının fiziksel özelliklerinin madde püskürmesi karşısında ortaya çıkan etkileri incelenmektedir. Bu doğrultuda, 2S 1417-624 adındaki değişen kaynakta 2018 yılında gerçekleşen dev madde püskürmesi ele alınmaktadır. Nötron Yıldızı İç Yapısı Kâşifi (Neutron Star Inner Composition Explorer) teleskobuna ait 1 Nisan ile 6 Eylül 2018 tarihlerinde bu madde püskürmesini kaydeden fırsat gözlemleri analiz için ele alınmıştır. Analiz süreci, madde püskürmesi etkilerinin doğrudan doğruya etkin olduğu bütüncül bir ışık eğrisini içermektedir.

Zamansal analiz için buna ek olarak, kaynağa ait dönme periyodu yaklaşık 17.4 saniye olarak ölçülmüştür. Bu değer güç tayfı ve dönem katlama aracılığıyla da net bir biçimde görülebilmektedir. Her bir gözleme ait güç tayfı teker teker incelenirken, bir tanesinde 1 Hz civarında marjinal bir Yarı-Periyodik Salınım gözlemlenmektedir. Dönem katlama aracılığıyla elde edilen faz profilleri, parlaklık değişkenliğinde madde püskürmesi kaynaklı bir değişim göstermiştir. Bu durum, akış geometrisinde bir değişikliğe işaret etmektedir. Bu sebeple bu tez, akış geometrisindeki bu değişimi daha

iyi anlamak amacıyla kaynağa ait her bir gözlemin tayfsal özelliklerinin değişimini incelemektedir. Zamana bağlı çözümlenmiş tayfsal parametreler, Hidrojen sütunu ışık akısı ile neredeyse tamamen hizalanmıştır ve dışarıdan gelen bir kısmi kapama etkisinin varlığını göstermektedir.

Güç yasasına ait foton indisi ile parçalı kapamaya ait kapama kesiti benzer evrimsel özellikler göstermektedir ve bu ilişkisel kurulumlar, süper-kritik parlaklık bölgesine erişildikçe ortaklaşa bir şekilde değişimle sınırlanmış durumdadır. Lakin, akış rejiminde yer alan tüm bu tayfsal parametre değişimleri 12 keV altında yeterince güçlü görünmemektedir. Fakat, akı ile çözümlenmiş tayfsal parametre evrimi, foton indisi bakımından önceki madde püskürmeleriyle tutarlı sonuçlar içrmekte ve ayrıca var olduğu önerilen kısmi kapamanın fiziksel yapısıyla birlikte akış geometrisinin akı arttıkça tecrübe ettiği dönüşümü açıklamaya yardımcı olacak detaylar sunuyor.

Anahtar Kelimeler: nötron yıldızları, X-ışını çiftlileri, emilim diskleri, 2S 1417-624

to my dear grandpa who is now with Ayvalık breeze and my mum, light of my life

ACKNOWLEDGMENTS

First and foremost, I am immensely grateful to my Supervisor and mentor Prof. Altan Baykal for introducing me to this beautiful field and providing me the necessary capabilities to make me one step closer for becoming a high energy astrophysicist. Likewise, I am very grateful to my co-Supervisor Dr. M. Miraç Serim for spending countless hours, patiently teaching innumerable amount of skills from his infinite bounty. Every conversation and scientific work I had with Dr. Serim has been enlightening and worth remembering. I am grateful to Prof. S. Çağdaş İnam for contributing to my academic career with his insight and being with me as a mentor since the time I started studying with METU High Energy Astrophysics Team (HEAT). This insight is provided to me by Dr. Şeyda Şahiner as well and I am thankful to Dr. Şahiner for all the life and academic guidance. I would like to thank my friend and fellow group member Çağatay Kerem Dönmez for all the technical support and educating me with valuable python skills. I would also like to thank the rest of METU HEAT Group Members Dr. Danjela Serim and Fatma Yaşa for being my colleagues. Finally, I would like to thank Sılanur Sevgen for designing fantastic artist depictions of all the astrophysical sources I have worked with and designing our group logo.

I acknowledge the TÜBİTAK Scholarship MFAG 118F037 which funded this thesis. I also would like to thank METU Physics Department and the Astrophysics Division as all of the scientific content of this thesis were made by using the "ASTROD" server.

Furthermore, I thank Ekincan Şimşek for never letting me go while learning to fly, in my time of rajaz echoes. I also thank Özgün Kum, Aylin Tuncalı, Ege Eryazgan, Ld. Ekin Özüdoğru, Ömer Sözer, all the members of ODTÜ AAT, ISEC team and all my friends whose names are written in my heart instead of this paper for being with me encouraging me to pursue my dreams, for being my past, present and future. Finally, I cannot thank enough to my family for always being there for me unconditionally. While writing this thesis I was shaken by the loss of my dear beloved grandfather Kazım Kabakçı and my cat sister Hürroş. Their memories will live on in me.

TABLE OF CONTENTS

ABSTRACT v

ÖZ vii

ACKNOWLEDGMENTS x

TABLE OF CONTENTS xi

LIST OF TABLES xiv

LIST OF FIGURES xv

CHAPTERS

1 INTRODUCTION 1

1.1 Theory 1

1.1.1 Physical Definition and Properties of Neutron Stars 1

1.1.2 Pulsars 3

1.1.3 High Mass X-ray Binaries 4

1.1.3.1 Be Type X-ray Binaries 7

1.1.4 Statistics of Analyzing an Observation 9

1.1.4.1 Spectral Model Fitting: χ^2-test 9

1.1.5 Definitions of Statistical Models Applied 10

1.1.5.1 Photon Absorption 10

1.1.5.2 Power-Law 11

1.1.5.3 Partial Covering Absorption 13
1.1.5.4 Gaussian Iron Line 14
1.1.6 Power-Density Spectrum 16
1.1.6.1 Quasi-Periodic Oscillations 17
1.2 Instrument: NICER 18
1.3 2S 1417-624 19
1.4 The Outline of the Thesis 21
2 ANALYSIS AND RESULTS 23
2.1 Observation Selection 23
2.2 Data Reduction 25
2.3 Timing Analysis 26
2.3.1 Total Light Curve 26
2.3.2 Power Spectrum 27
2.3.2.1 Marginal QPO 28
2.3.3 Spin Period Measurements 31
2.3.4 Pulse Profiles 32
2.4 Spectral Analysis 34
2.4.1 Background Reduction and Calibration 34
2.4.2 Model Selection 35
2.4.3 Spectral Evolution 37
2.4.3.1 Preliminary Analysis 38
2.4.3.2 Consequent Analysis 39
3 DISCUSSION AND CONCLUSION 43

REFERENCES 49

LIST OF TABLES

TABLES

Table 2.1 NICER TOO Observations that were used in this thesis 24

LIST OF FIGURES

FIGURES

Figure 1.1 Typical representation of the interior of a $1.4M_{\odot}$ neutron star . . 2

Figure 1.2 Physical representation of a rotating and magnetized neutron star. 4

Figure 1.3 Very first observational light curve of a pulsar 5

Figure 1.4 Representation of the basic schematics of a magnetized neutron star where Alfvén Surface, radius and X-ray beams from the poles are visible. 7

Figure 1.5 Schematics describing how a neutron star facilitates a periastron passage and thus generates an accretion disk and finally accretes all the absorbed material from the circumstellar disk of the companion star . . 8

Figure 1.6 Physical representation of the inverse compton scattering process, main reason of the majority of X-ray emissions in X-ray Binaries. Figure Credit: Chandra X-ray Observatory, Harvard University. 12

Figure 1.7 Representation of a Neutron Star where the regions of which several types of Comptonisation is shown. Bulk and Thermal Comptonisation processses are thought to be the main source of observing power-law spectra in X-ray binaries. 13

Figure 1.8 A very simple Gaussian with width of 0.01 amplitude generated in python numpy. 14

Figure 1.9 A Bohr Atomic Model description visually describing the K, L and M shell electrons and emission line generation in the Iron Atom . . 15

Figure 1.10 A visualization that represents a power spectrum 18

Figure 1.11 A photograph of the NICER telescope where its Silicon Drift Detectors are clearly visible 19

Figure 1.12 Comparison between the effective ares of NICER and XMM-Newton 20

Figure 1.13 Artist's Interpretation of 2S 1417-624. Image Credit: Sılanur Sevgen 21

Figure 2.1 Total Light Curve of 2S 1417-624 During its 2018 giant outburst 27

Figure 2.2 Power spectrum of 2S 1417-624 generated from the combined NICER light curves of the whole 2018 outburst 28

Figure 2.3 Power spectrum of Obs. ID. "1200130123" 29

Figure 2.4 Power spectrum of ID. "1200130126" 30

Figure 2.5 Upper Panel: Power spectrum where the strongest feature of the marginal QPO is shown. The line shows the model continuum which, alongside with the analytical details of the power spectrum is described in the main text of this section. Lower Panel: A sigma test that was applied to this continuum in the upper panel. The peak of the marginal QPO shows a deviation from the continuum with the significance level of 1.67σ. 31

Figure 2.6 The spin period search result of 2S1417-624. The central peak at the origin clearly shows the best period at 17.465 with a resolution of 0.01. 32

Figure 2.7 Pulse profile of 2S 1417-624 just before the outburst 33

Figure 2.8 Pulse profile of 2S 1417-624 right at the peak of the outburst . . 33

Figure 2.9 Pulse profile of 2S 1417-624 right after the outburst 34

Figure 2.10 An example spectrum of 2S 1417-624 fitted with the model configuration involving partial covering fraction absorption. OBSID: 120130123 36

Figure 2.11 Results of the preliminary spectral evolution where parameters shown provide little to no variation. 37

Figure 2.12 Resulting spectral evolution of the preliminary analysis with Blackbody model. 39

Figure 2.13 Time resolved spectroscopy of 2S 1417-624 with PCAF model applied alongside with previous configurations where as an addition, parameters that show no change are fixed. 40

Figure 2.14 Flux resolved spectroscopy of 2S 1417-624 with PCAF model applied alongside with previous configurations where as an addition, parameters that show no change are fixed. 41

Figure 3.1 Pulse profiles of 2S 1417-624 generated with NuStar(Red) and RXTE(blue) observations after the peak of the outburst where a double peak structure beyond the critical luminosity is visible. This figure is directly taken fromfrom Gupta et al. (2019)[16]; Figure 2 45

CHAPTER 1

INTRODUCTION

1.1 Theory

1.1.1 Physical Definition and Properties of Neutron Stars

Massive stars have distinctive evolutionary processes which yield the conditions for formation of a neutron star. Neutron stars (NS) are the residual cores of massive stars after they go through a core-collapse supernova. During this stage, the gravitational pull of massive stars overcomes the hydro-static equilibrium and the atoms making core of massive stars start to squeeze in such extreme levels that protons which used to be a part of the core lose their atomic integrity and turn into neutrons by a series of inverse β decays which is shown in Equation 1.1. Such process can only occur if the density of the environment provides the stage for the electron gas provides significant special relativistic effects[26].

$$p + e^- \rightarrow n + \nu_e \tag{1.1}$$

Inverse β decay process

Protons in the cores of massive stars which are nominally stationed in a cloud of non-degenerate electron gas and therefore even if an inverse β decay occurs in normal circumstances, almost immediately after the neutron resolves into protons and electrons. In order for this process to occur irreversibly, there must be no possible energy levels for a generated electron to be stationed at and as a consequence become degenerate. Should, due to the heavily increasing density of the core, such an instability occurs, then a neutron-rich nucleus forms from this initial stellar core in a chain

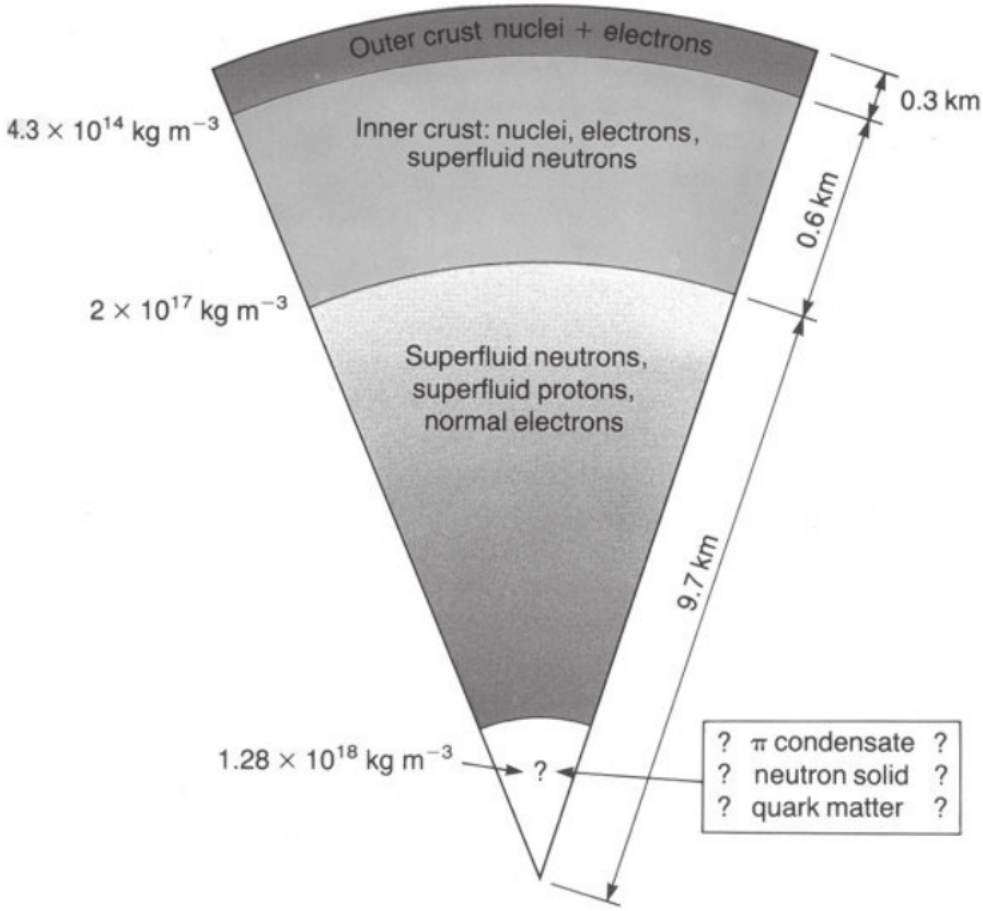

Figure 1.1: Typical representation of the interior of a $1.4M_{\odot}$ neutron star. Figure taken from: fig 13.13 of "High Energy Astrophysics" by Malcolm Longair 2nd edition[27]

.

reaction of inverse β decays, a process sometimes called as *neutronisation*. These so called *proto-neutron stars* start to gather new neutrons for their nuclei with a central density of $10^{10}kg/m^3$ and this process of richening the nuclei via neutronisation continues up until the density reaches to a level around $4 \times 10^{14}kg/m^3$ after which neutron-rich nuclei can no longer station new neutrons the neutron star initiates the outward release of neutrons, a process commonly named as *neutron drip*[27]. After the neutron drip process is reached, entirety of the materials that once formed the massive star becomes a bulk material almost full of only neutrons(see Figure 1.1) and this newly generated neutron pressure does not allow gravitational potential energy to collapse further and a relative stability, an equilibrium is reached at around $10^{17}kg/m^3$.

In the most general sense, the physical properties describing white dwarfs could also be applied into neutron stars by considering the fact that neutrons are around 2000 times more massive than electrons. However, physically describing neutron stars also require some general relativistic effects to be taken into consideration due to the extreme densities of their cores which are sufficiently high enough to show noteworthy general relativistic effects[27]. This innermost regions of the neutron stars which generate significant general relativistic effects are not very well explained due to the difficulties of both acquiring new information from such extreme regions and difficulties regarding calculating proper equations of state for such degenerate nuclear matter[39]. Models used to describe the inner structures of neutron stars usually do not take these innermost regions into account and types of matter which are exotic to the common knowledge is thought to exist especially in massive neutron stars with mass larger than 2 $M_{\odot}$. Additionally, neutrons neither attract nor repulse each other due to lack of electromagnetic forces they apply to the universe[9]. Therefore, this situation, an neutron-rich sphere with enormous size, allows nuclear forces that commonly show their effects on the atomic nucleus to be taken into account.

1.1.2 Pulsars

Since neutron stars are in fact the remnants of massive stars, they are constrained by all the conserved quantities of their progenitors, such as angular momentum. These initial conditions cause neutron stars to directly inherit the rotation of their progenitor stars due to the conservation of angluar momentum. Additionally, flux conservation triggers emitted flux to increase rapidly due to the sudden decrease in the size of the newly formed neutron star compared to its progenitor. This phenomenon makes the newly formed neutron star to inherit large amounts of magnetic field compared to the relatively low magnetic field values of its progenitor star. It is also vital to point out that electrons existing at the interior regions of the neutron star create magnetic dipole forms along the rotational axis which in turn contributes to the overall magnetic field of the neutron star. The magnetic field causes some outer charged particles to flow towards the magnetic poles and heat up these poles of the neutron star, which in turn provides beams of light -pulses- to be regularly transmitted from the poles of the neutron star. Such neutron stars radiate away series of regular pulses as they rotate

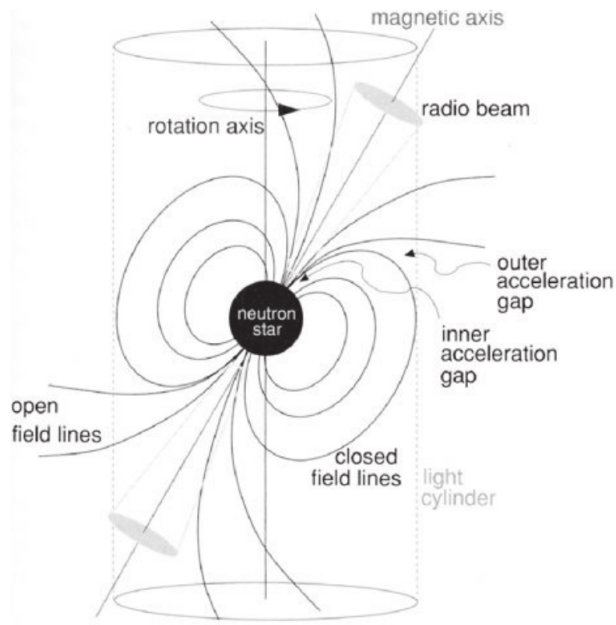

Figure 1.2: Physical representation of a rotating and magnetized neutron star. Figure Credit: Fig 13.15 of "High Energy Astrophysics" 2nd Edition by Malcolm Longair[28]

and are called *pulsars*. First observation of a neutron star was made by Jocelyn Bell Burnell. This initial observation was a series of radio pulses being emitted from the source (Hewish et al. 1967[19])(see figure 1.3). Pulsars typically inherit around 10^{12} G magnetic field and this extremely high magnetic field is the main source of power for its pulses. These pulses can happen due to magnetic breaking creates a reduce in the kinetic energy which in return emitted as magnetic dipole radiation. Such pulsars are called *rotation powered pulsars*. Depending on the environmental conditions (being in a binary system and/or surrounded by material), some pulsars create their pulses due to the acceleration of an external storm of charged particles, a process called accretion. These pulsars are called *accretion powered pulsars*.

1.1.3 High Mass X-ray Binaries

Most of the observed neutron stars in the universe are within binary systems. Chemical and physical interactions that produce emissions of light or gravitational waves occur more commonly in a physical system consisting external material and astro-

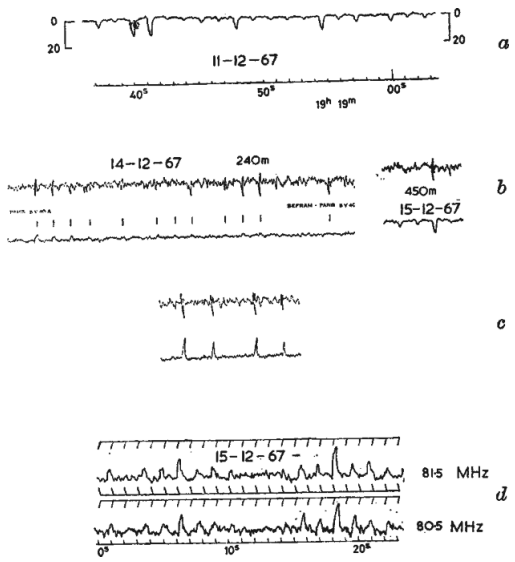

Figure 1.3: Very first observational light curve of a pulsar. Credit: Hewish et al. (1967) [19]

nomical source. When a neutron star gravitionally attracts an ordinary star or a body of mass, they share a mutual binary orbit with the neutron star and afterwards it starts to steal material from external objects, either via Roche lobe overflow or stellar wind, depending on the physical conditions of the binary system. Stars are not always in hydrostatic equilibrium and they do not produce energy equally homogeneously throughout their surfaces. This means sometimes some regions of a star will be imbalanced. In order for this imbalance in height and energy to be compensated, star sometimes shoots out materials as either in terms of stellar wind or sometimes even a storm. Since the single-most greatest gravitational attraction towards the star is its companion neutron star, this generated stellar material directly arrives to the neutron star and creates a temporary acceleration disk in some neutron stars or a spherical accretion may occur after the formation of a shock along the Bondii radius[8]. While the flow of material occurs towards the neutron star, this flow is disturbed by the effects of the magnetic field which carries these particles to the poles along the magnetic field lines. Afterwards, these charged materials heats up certain regions at the magnetic poles along the rotational axis of the neutron star. This process creates an overly heated region around these poles due to excessive material impact and these regions are commonly named as *hot spots*. Stars with high masses commonly produce or generate stellar winds and these process described above is the nominal physical

process happening in *high mass X-ray binaries*. However, it is also worthy to note at this point that a very similar process also occurs when a star with large mass forms a binary orbit with a black hole and it is very challenging to distinguish the nature of the compact object initially. Therefore it is safe to define that a High Mass X-ray Binary(HMXRB) is a binary system consisting of a high mass star and a compact object, namely a neutron star or a black hole. It is also noteworthy to state that the beams of light do not always occur by all the pulsars. The main determining factor for these pulsations to occur is the strength of the magnetic field which should be sufficiently high enough to interrupt the matter flow process to the pulsar surface. The determining factor for this magnetic field strength is the radius of the magnetostatic region of the pulsar. If this radius is smaller than the radius of the pulsar itself, then naturally no magnetic field exists to interrupt the matter flow process as funnelling. This magnetic field radius is determined by *Alfvén Radius* (r_A) as shown in the Equation 1.2:

$$r_A = \sqrt[7]{\frac{\mu^4}{2GM_\star^2\dot{M}}} \tag{1.2}$$

Where;

- μ is the magnetic moment
- G is the gravitational term commonly named as Newton's Gravitational Constant firstly introduced in the Law of Universal Gravitation or Kepler's Third Law. In the CGS units, the constant is defined as $6.6743 * 10^{-8} cm^3 g^{-1} s^{-2}$.[34],
- $\dot{M}$ is the accretion rate commonly denoted as the time derivative of mass, the units of this parameter is solar mass per year.
- $M_\star$ is the pulsar of the source in solar mass.

It should also be noted that this term is the radial component of an Alfven surface generated by the magnetic field. If the radius of the pulsar "r" is smaller than r_A, then magnetic funneling occurs and neutron star generates such magnetic pulses. On the other hand, if r_A < r, matter directly falls into the surface of the pulsar[31]. General overview of wind accretion schematic is illustrated in Figure1.4.

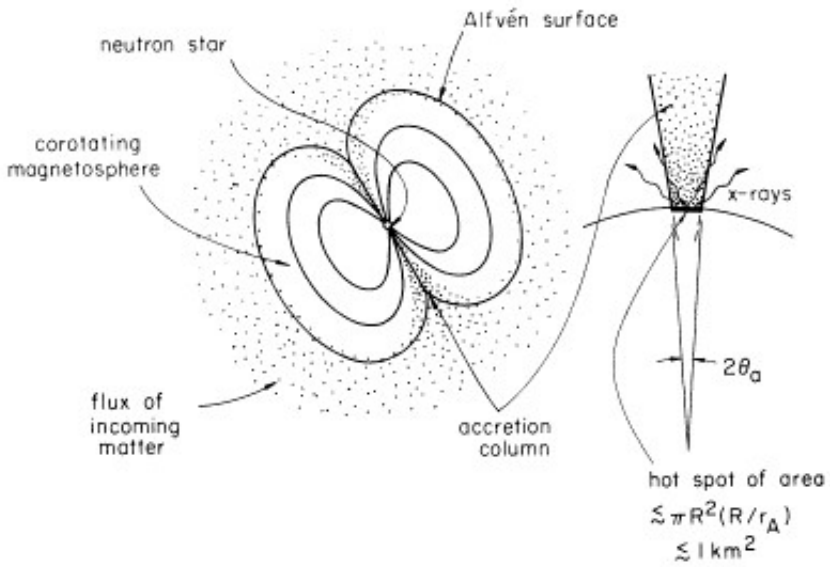

Figure 1.4: Representation of the basic schematics of a magnetized neutron star where Alfvén Surface, radius and X-ray beams from the poles are visible. Sketch taken from "Fig1" of Lamb et. al. (1973).

1.1.3.1 Be Type X-ray Binaries

HMXRBs consists of massive stars, namely O or B type. Such class of stars are extremely unstable due to their nature and consistently throw away stellar material from their outer layers in forms of stellar winds. Stars of B spectral type usually rotate really fast and this rotation produces hotter wind material compared with O type stars. Due to this heavy rotational behavior, the outflowing material created a *decretion disk* which creates a torus shape around the star as a *circumstellar disk*. This extreme, yet curiously mysterious rotation property is the main distinguishable factor for classifying a star "Be-type" and such compact binary systems-ones that contain a Be-type star- are called *BeX-ray Binaries(BeXRBs)* The flow of material generated by the Be-type star is then absorbed by the pulsar through the process mentioned above which in turn provides series of outbursts as the pulsar is fed by this flowing material. The accretion occurs when the pulsar enters the decretion region of the Be-type star and as a result, the pulsar "gathers" a bulk of material from this circumstellar disk of the Be star and that newly generated accretion disk of the pulsar is the main fuel of outbursts. Such outburst activities generated by BeXRBs generally create series of

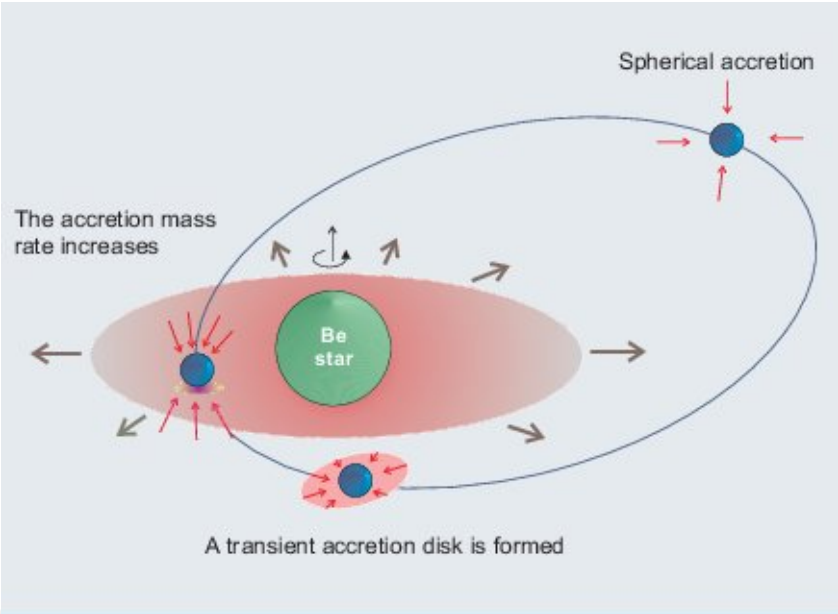

Figure 1.5: Schematics describing how a neutron star facilitates a periastron passage and thus generates an accretion disk and finally accretes all the absorbed material from the circumstellar disk of the companion star. Figure Credit: Orellana et al. (2004)[35]

gradual increase and decrease in X-ray flux due to high amounts of X-ray emission produced by these heavily charged particles which were once a part of the stellar wind of the Be-type star. These extremely bright outburst events are usually observed by the telescopes as a "Target of Opportunity" occurrence. Some outbursts in BeXRBs occur somewhat regularly, such outbursts generally last relatively shorter and they are thought to happen during the periastron passage of the pulsar and therefore investigating the pulse profiles that are created by these sources during times of the outbursts are highly useful. These outbursts are called *Type I Outbursts* and they usually acquire an X-ray flux with maximum value of 10^{37} ergs s^{-1}[35]. There are also some outbursts that occur in a chaotic and irregular sense. They usually last relatively long and their intensity are higher than Type I outbursts. These *Type II outbursts* create extremely bright flares that reach the physical limit of luminosity a neutron star may have, the *Eddington Luminosity*. When this luminosity limit is reached, the pulsar does not allow the outer material to fall into its surface anymore and radiation pressure overcomes the gravitational pressure. The physics behind taking Eddington Luminosity

as an upper limit for neutron star luminosity is based on the useful assumption that the main producing factor of X-ray flares in such sources is Thomson Scattering. The Eddington Luminosity "L_{Edd}" is mathematically described as the equation1.3.

$$L_{Edd} = 1.2 * 10^{38} \left(\frac{M_\star}{M_\odot} \right) \text{erg/s} \tag{1.3}$$

Where "$M_\odot$" is the mass of the Sun.

1.1.4 Statistics of Analyzing an Observation

1.1.4.1 Spectral Model Fitting: χ^2-test

Observational astronomy relies on producing relevant statistical models that physically describe the source in the most convincing way. In order to understand this degree for being a model combination to be convincing, model fittings are considered in terms of statistically accuracy. Physically relevant model combinations are first determined and then fitted to the observational data to be observed, e.g. a spectrum. Upon all the model candidates and physical explanations, the best fit model is then determined via χ^2*-test*.

χ^2-test or *chi-squared test* is one of the most determining statistical tools to understand if a model fit is statistically significant enough to physically describe the observational data of an astronomical source and used very commonly especially in X-ray spectral analysis. Introduced firstly by Karl Pearson[36], the concept relies on the ratios of the differences of the expected and observed values as shown in equation 1.4

$$\chi^2_f = \sum_i^N \frac{(O_i - E_i)^2}{E_i} \tag{1.4}$$

Where;

- f is the degrees of freedom, obtained by subtracting the number of data points from the number of model parameters.

- O_i is the observational data for every i^{th} data point
- E_i is statistically envisaged value for every i^{th} data point
- N is the total number of data points.

The value "χ_i^2" is generally divided by the degree of freedom in order to acquire *Reduced* χ^2 and it should ideally approach to 1. Any value of the reduced χ^2 between 0 and 1 is an indication of a model being over-fit and any value above 1 means the degree of which model deviates from the observational evidence.

1.1.5 Definitions of Statistical Models Applied

In this section, some of the most commonly used models for explaining the physics of compact objects will be mentioned. More details on how are these models applied to the observational data will be mentioned in the following Chapter at Section 2.2.

1.1.5.1 Photon Absorption

No astronomical light arrives to our telescopes without some level of interference with the interplanetary, interstellar and intergalactic space, where various external sources such as optically thin bodies of mass, clouds of gas or simply background noise can cause the incoming light from the intended source to be analyzed lose information and get distorted via series of absorption. Since this phenomenon is a priori assumed exist at least in forms of basic background absorption of hydrogen gas, this model is the baseline of every other model combinations and it is always taken into account. This model is represented as the equation 1.5[1] :

$$M(E) = e^{-\eta_H \sigma(E)} \tag{1.5}$$

Where:

- (E) flux as a function of energy.
- e is the exponential constant

[1] https://heasarc.gsfc.nasa.gov/xanadu/xspec/manual/XSmodelPhabs.html

- η_H or N_H is the Hydrogen column density of the background. The unit of this parameter is 10^{22} atoms per cm^2. The matter accumulated between the Earth and any object in the universe to be observed is most generally Hydrogen. Even thought there would be other clouds of matter, there will always be some forms of existing Hydrogen to be reduced from the observation. This accumulation of Hydrogen is conventionally called a *Hydrogen Column* and these columns make incoming photons go through a form of extinction that should be reduced when analyzing a source. This galactic extinction and N_H are linearly correlated.[17]

- $\sigma(E)$ is the cross-section of the surfaces on which photo-electric absorption takes place.

1.1.5.2 Power-Law

In the most general sense, power-law is the overall link of different physical parameters in terms of an exponential sense such that if two parameters are connected to each other with a power-law, then if one component increases or decreases, the other will also increase or decrease but with a degree of some power.[5] Power-law is a widely observed model in all areas of science and the statistical model describing power-law is the basic principle for modelling the spectra of neutron stars. Observations and spectral analysis of neutron stars and X-ray binaries since 1970s consistently show suitable fit to Power-Law spectral model[22] shown in equation 1.6 taken from NASA HEASARC[2].

$$M(E) = KE^{-\alpha} \tag{1.6}$$

Where

- α or Γ is the *photon index*, a dimensionless parameter that is used to calculate the exponent of the energy dependence of the flux density.

- K is the normalization parameter in units of photons(or counts) per keV per cm^2 for 1keV

[2] https://heasarc.gsfc.nasa.gov/xanadu/xspec/manual/XSmodelPowerlaw.html

- M(E) is the flux density as a function of energy. E in this overall model is the given energy of each photon.

It noteworthy to point out at this stage that power law have some variations such as *broken power law* or *smoothly broken power law*. This implies that under some circumstances, power law component does not necessarily need to be extend to all energy range and some breaks may occur due to physical external contributions.

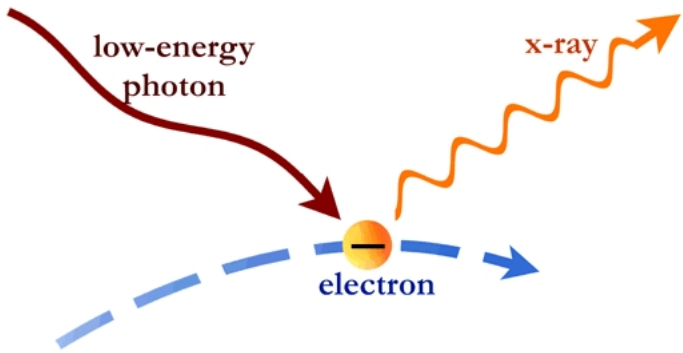

Figure 1.6: Physical representation of the inverse compton scattering process, main reason of the majority of X-ray emissions in X-ray Binaries. Figure Credit: Chandra X-ray Observatory, Harvard University.

Source of Power-Law Spectrum in Neutron Stars; Inverse Comptonisation Regardless of the sources of accelerated electrons or photons that interacted on a region close to the neutron star, the series of inverse compton scatterings occur and this comptonisation process can only happen or diminish exponentially because of the accelerated radiative nature of the incoming electrons. The distribution of the series of exponential emissions is explained by the statistical model of the power law. This is the most inferential and elementary reasoning explaining why power law is observed in the X-ray spectra of pulsars.

The main discussion starts on the location where these accelerated electrons are created of these accelerated electrons and the materials surrounding the neutron star. Although the main reason behind observing a power-law in the spectra of pulsars is still unknown to this day, the most widely accepted explanation comes from the so

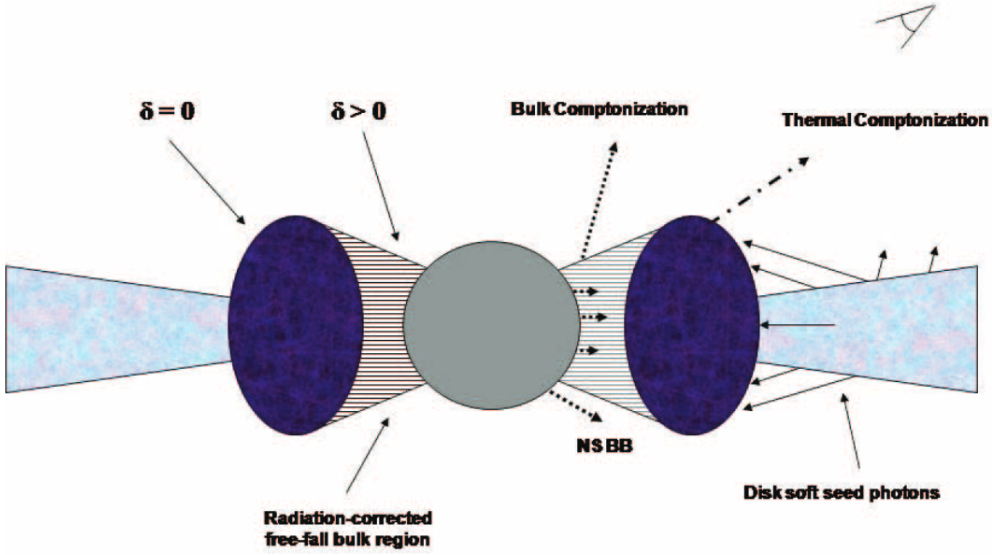

Figure 1.7: Representation of a Neutron Star where the regions of which several types of Comptonisation is shown. Bulk and Thermal Comptonisation processses are thought to be the main source of observing power-law spectra in X-ray binaries. Figure Credit: Farinelli et al. (2008)

called "Disk Accretion Model" of Ghosh & Lamb[14]. The Ghosh & Lamb model discusses about the existence of hot bodies of bulk material consisting of electrons that are heavily effected by the beam of light generated by the magnetic and gravitational effects which in turn generates a cycle of inverse comptonisation, a process created by series of inverse Compton scattering as shown in figure 1.6

1.1.5.3 Partial Covering Absorption

Partial Covering Fraction Absorption (PCFABS) is essentially an enhanced version of a nominal photon absorption model mentioned at 1.5. However, PCFABS does not represent the galactic background noise but rather an existing bulk material whose fraction of some degree covers the object to be observed and as a consequence interferes with the analysis. This bulk material is also assumed to be a Hydrogen Column with some N_H but a degree of covering fraction; f is also needed to be taken into account. PCFABS model is described by the following Equation 1.7 taken from NASA

HEASARC manual[3].

$$M(E) = fe^{\eta_H \sigma(E)} + (1 - f) \tag{1.7}$$

M(E), η_H and $\sigma(E)$ are the same parameters described at 1.5 with an addition of f where that is the partial covering fraction, a dimensionless parameter between zero and one, used in order to describe how much of the source is covered by the bulk material.

1.1.5.4 Gaussian Iron Line

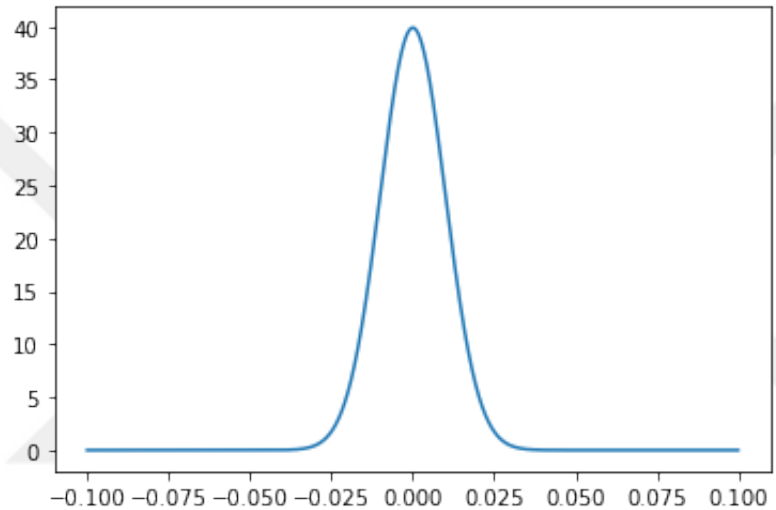

Figure 1.8: A very simple Gaussian with width of 0.01 amplitude generated in python numpy.

Gaussian(GAU) Iron Line is a Gaussian structure usually added to an overall model combination to describe emission lines. In X-ray astronomy, GAU is most commonly used for taking Iron(Fe) line into account. Fe atoms are mostly originated from the supernova event occurred in the progenitor of the pulsar and stationed at the disks of X-ray binaries. Therefore when any extracted photon spreads towards that disk, it excites the Iron in the disk in a form of reflection. This photoelectric effect produces several emission lines in Fe of which the strongest being Fluorescent(K_α line). This line nominally exists at 6.44 keV Energy level and its broadness(width being high equivalent width) implies a high intensity of light and therefore an abundance of Iron

[3] https://heasarc.gsfc.nasa.gov/xanadu/xspec/manual/node258.html

in the disk[29]

Gaussian line could be used for describing any atomic emission line in an observational model. However, the scope of this thesis only focuses on the usage of

$$A(E) = K\frac{1}{\sigma * \sqrt{2\pi}}e^{\frac{-(E-E_l)^2}{2\sigma^2}} \tag{1.8}$$

Where

- M(E) is the spectrum of Energy E
- E_l is the central energy of the emission line
- K is the total number of photons per cm^2 s in the line at E_l
- σ is the width of the emission line centered at E_l

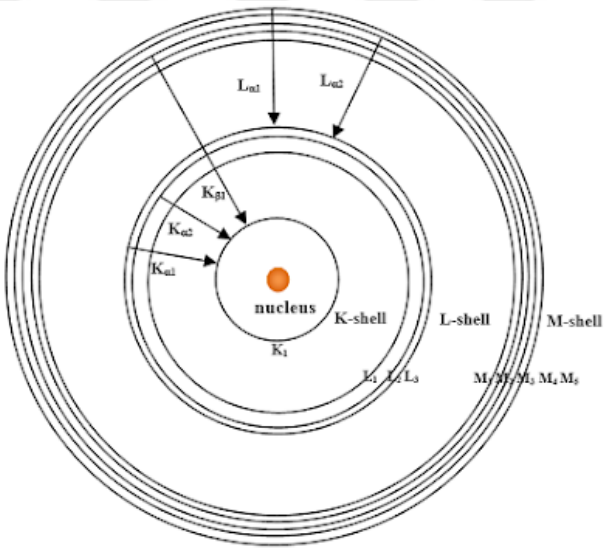

Figure 1.9: A Bohr Atomic Model description visually describing the K, L and M shell electrons and emission line generation in the Iron Atom

GAU for Fe K_α line. GAU model -and in this case any Gaussian Normal Distribution- could be described by equation 1.8 taken from NASA HEASARC[4]. There are some variations to the Gaussian curve such as a *Lorentzian*. Such curves are obtained by

[4] https://heasarc.gsfc.nasa.gov/xanadu/xspec/manual/node176.html

breaking the symmetry in the ordinary Gaussian by some direction and degree so that either the peak structure rapidly increases and/or decreases.

1.1.6 Power-Density Spectrum

All pulsars and XRBs are variable sources and they produce this variability of different parameters in time needs to be investigated according to their regularities. Pulsars are inherently oscillating sources and any irregularities in these oscillations in their light-curves are treated in a signal processing sense of electrical engineering. Therefore one of the most common tools to investigate the timescales of a pulsar is to test the variability of the oscillations. The important point is to distinguish regularities of these inconsistencies and being able to distinguish them from the overall background noise. Therefore it is vital to determine the strength of each regular inconsistent signals. One of the most conventional ways to determine this "power" is to first consider light-curves as a series of several sinusoidal signals and let it go through a Fourier Transformation and then normalize this Fourier Transformation by some parameter that is the total number of photons acquired from the signal. This averaged time intervals that turn into a power spectrum is vital for making the statistical significance of the spectrum attributes[40]. This basically allows researchers to investigate a signal not in the time-domain as in the light-curve but rather in *frequency-domain* as in the *power spectrum*. The Fourier transformation of any signal could be written as equation 1.9

$$A_j = \sum_k x_k cos\omega_j t_k \;\; \& \;\; B_j = \sum_k x_k sin\omega_j t_k \tag{1.9}$$

This Fourier transformation can be applied to a time series of x_k where k is the each measurement due to time i.e. k=0,...,N-1. For such a configuration, the parameter j becomes the time window that can be expressed as the following: $\forall k \in Z \Rightarrow -N/2+1 \leq j \leq N/2$. Now, by making use of the inherent property of the exponential expressions of trigonometric functions, one can write an imaginary expression of the Fourier transform as the following:

$$A_j = \sum_{k=0}^{N-1} x_k e^{2\pi ijk/N} \;\; \& \;\; x_k = \frac{1}{\sqrt{2\pi}} \sum_{j=-N/2+1}^{N/2} a_j e^{-2\pi ijk/N} \tag{1.10}$$

Notice here that frequency term is for a circular period such that

$$w_j = 2\pi\nu_j = \frac{2\pi j}{T} \tag{1.11}$$

Where T is the overall time window under the location j such that the term ν_j becomes in a way the circular velocity. Since both of the expressions in equation 1.10 is imaginary, it is possible to argue about a power of which is created after a normalization process that makes these Fourier transformation expressions real. Taking this and Parseval Theorem[2] into account provides us the expression in Equation 1.12:

$$\sum_k x_k^2 = \frac{1}{N}\sum_j |a_j|^2 \tag{1.12}$$

If the expression $\sum_k x_k$ is considered as the total number of photons in time series, i.e. N_{ph}, then a parameter called **Power Spectrum;** P_j which can be defined as the following: 1.13

$$P_j \equiv \frac{2}{N}|a_j|^2 \tag{1.13}$$

Finally, transcribing these sum expressions into the frequency space provides us the conventional definition of the power density spectrum: 1.14

$$\sum_{j=j_1}^{j_2} P_j = \int_{\nu j_1}^{\nu j_2} p(\nu)d\nu \tag{1.14}$$

This expression means, instead of considering each individual data points separately and summing them one by one, an infinite sum of numerous parameters of infinite changes in frequency as a form of an integral. A more enlightening figure can be found at figure 1.10. This overall derivations are part of a larger lecture by Michiel van der Klis[41].

1.1.6.1 Quasi-Periodic Oscillations

Power spectra is most commonly used in order to determine unusual behaviors in a very regular stream of x-ray pulsar photons that form a light curve. Sometimes, in addition to these regular pulsations, light curve may include some other oscillations of alterations. Investigating a light curve in frequency domain allows researchers to detect such chaotic semi-regular flares or abnormal attitudes of the source. Such marginal occurrences are commonly referred as *Quasi-Periodic Oscillations(QPOs)*[30].

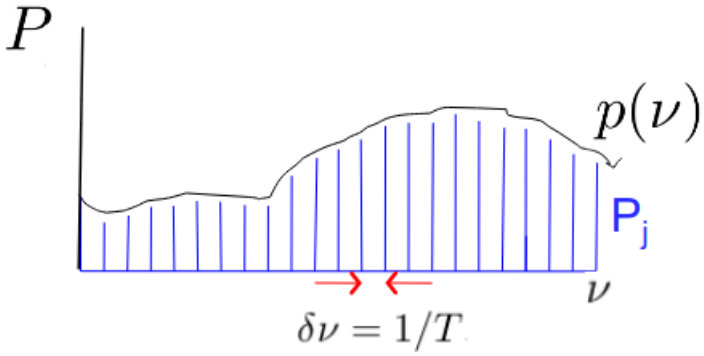

Figure 1.10: A visualization that represents a power spectrum. Image taken from van der Klis, 2010[41].

QPOs are thought to be originated due to irregular flow of mass to the accretion region of the neutron star and therefore creating marginal and abnormal flares which turn out to be semi-regular as this bulk mass will decay while rotating around the compact object[24]. The theory behind this section will be discussed further in Chapter 3.

1.2 Instrument: NICER

Neutron star Inner Composition ExploRer(NICER) is a space telescope operate in the X-ray waveband. It is stationed at the International Space Station (ISS) as an external payload that was launched in 2017 by Falcon 9 vehicle of SpaceX[13]. NICER provides extremely precise observations with high sensitivity X-ray detectors whose initial objective as the name suggests is to obtain clues from the interior parts of neutron stars as very little information in forms of photons arrive to our detectors. However, NICER already exceeded this goal and provided observations of X-ray binaries, AGNs, outbursts and novae. NICER is being operated in the soft energy ranges of X-ray waveband, namely between 0.2 and 12 keV. However, due to its low earth orbit, it is very susceptible to Earth-bound effects and ISS noise.[10] Therefore observations below 0.8 keV are deemed to be unreliable. The main scientific instrument used in NICER is its *X-ray Timing Instrument*(XTI) which is a large CCD-like structure with an array consisting 56 photon detectors sensitive in X-ray energy band. Each detec-

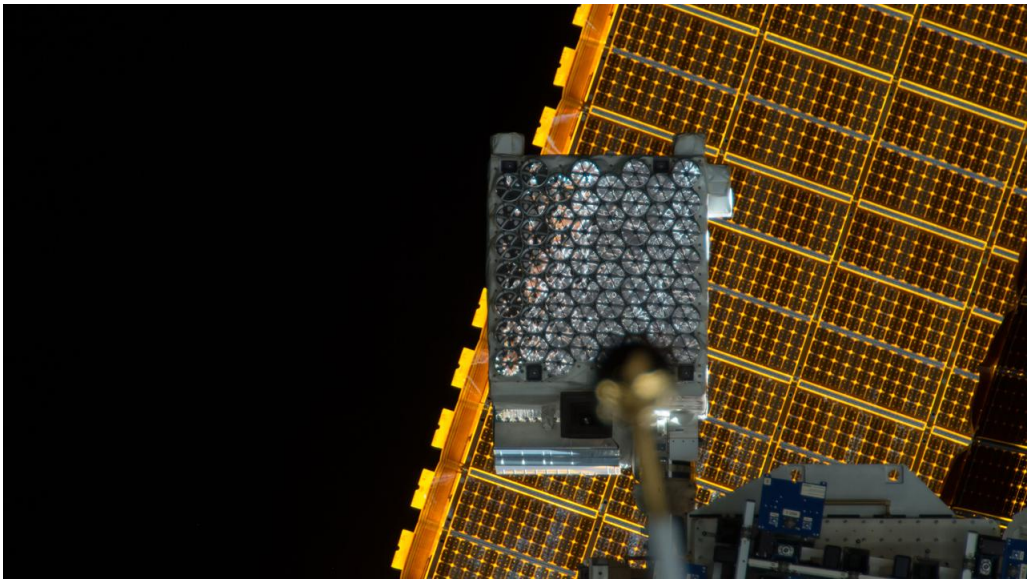

Figure 1.11: A photograph of the NICER telescope where its Silicon Drift Detectors are clearly visible. Image Credit: NASA

tor consists layers of silicon mirrors that trigger photoelectric effect and determines the frequency of incoming light according to the position of the excited photoelectric current flowing trough the corresponding semiconductor Silicon layer. Each layer of mirror is positioned with a slight angle which provides further accumulation of light into a more central location. These Silicon Drift Detectors possess the capability of detecting up to 100,000 counts per second. Sensitivity of each of these sensors is 600 ns. NICER data is either obtained through sending observation proposals or they are publicly accessible if the occurrence is a ToO observation. NICER is not designed to provide images of sources, instead the engineering capabilities were spent more on sensitivity of detectors and high resolution for spectroscopy and timing analysis. This choice in design allowed NICER to be 4 times more sensitive in detecting photons than XMM-Newton and to have 25 times higher resolution than RXTE.[3]

1.3 2S 1417-624

2S 1417-624(or 4U 1416-62) is a BeXRB positioned right next to the right toe of Centaurus Constellation whose coordinates in International Celestial Reference System and Frame(ICRS) being Right Ascension(RA): 14h 26m 12.8s and Declina-

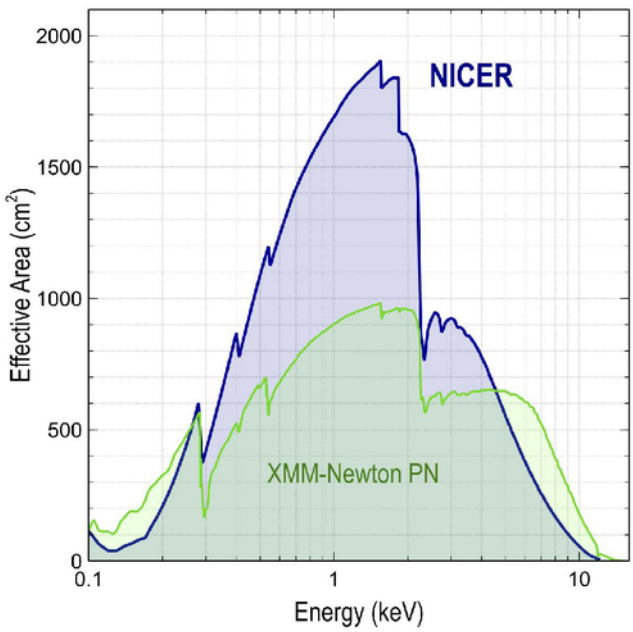

Figure 1.12: Comparison between the effective ares of NICER and XMM-Newton, more or less twice amount of difference implies four times high sensitivity. Image Credit: Gendreau et al. (2016)[3]

tion(DEC): -62° 41' 54" [12]. The discovery of 2S 1417-624 showed its transient nature by Small Astronomy Satellite 3 (SAS-3) as it was discovered while it was in a period of a giant outburst[1]. Although a rapid outburst and the companion star of the pulsar was observable in the visible waveband at that time, the pulsar with spin frequency of 0.5669 Hz was discovered in 1981[25]. The companion Be Type giant star was observed in optical band by Cerro Tololo Inter-American Observatory and these observations provided an identification B1 V*e* star with an apparent magnitude of 16.9 and an approximate distance between 1.4-11.1 kpc[15]. Later, Gaia survey made further observations and narrowed down the distance uncertainty in 2018 as 7.5-13 kpc[4]. On the other hand, torque accretion models seem to prefer rather large distances ($\sim$ 20 kpc; [23]). The *CGRO*/BATSE observed an outburst of 2S 1417-624 between August 1994 and July 1995 from which orbital period is found the be 42.19 days[20]. Another outburst of 2S 1417-624 was later observed between November 1999 and August 2000 allowed researchers to determine an eccentricity for the orbit of this source as 0.446[20]. Later, further outbursts of the source were observed in 2009 by *Fermi* Gamma-ray Burst Monitor (GBM)[7] and in 2018 by several observa-

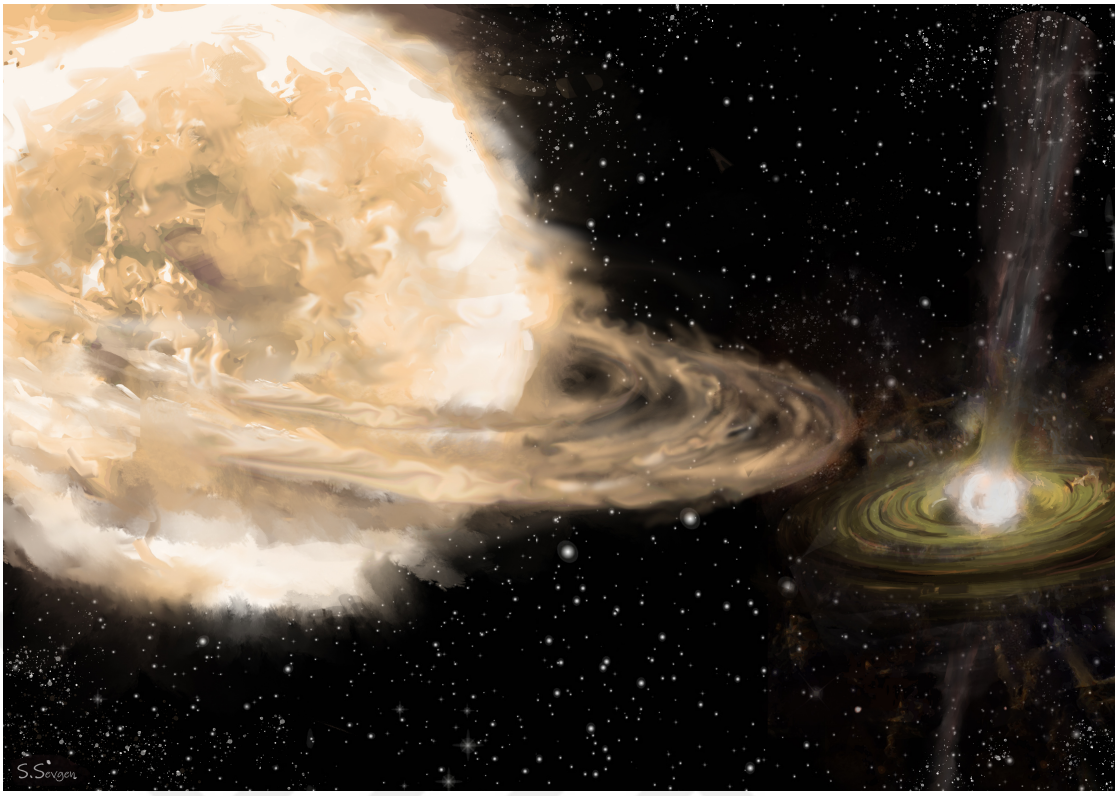

Figure 1.13: Artist's Interpretation of 2S 1417-624. Image Credit: Sılanur Sevgen

tories such as *MAXI*/GSC Nova-Alert System[32], *Fermi*/GBM, *Swift*/BAT and also *NICER*/XTI whose observations constitute the input data set of this thesis. Finally, last outburst from this source took place in 2021 which is monitored by *Swift*, MAXI and Fermi simultaneously[18]. It is very common for BeXRBs to maintain outburst properties since the neutron star orbits around a very unstable type of star, the passing of the neutron star from circumstellar disk of the companion star allows the accretion of vast amounts of material that provides an energy source for these giant outburst. 2S 1417-624 is known to go into an outburst stage frequently.

1.4 The Outline of the Thesis

Chapter 1 of this thesis provides the necessary theoretical, astronomical, statistical and instrumental background knowledge alongside with the overall outline of the content of this thesis. This knowledge includes physics of the formation of the neutron stars, inner and external content of a neutron star and definitions due to the nature of

the neutron star. Later, the thesis describes necessary astrophysics background such as pulsars and the binary systems defining 2S 1417-624. This description is further continued by the statistical tests used in the spectral studies of this thesis. Later, some relevant astronomical information regarding 2S 1417-624 is provided alongside with the instrumentation information of NICER.

Chapter 2 focuses on the data acquisition, reduction, methodology and analysis. The timing analysis of the source presents the total light curve, pulse period measurements by `efsearch`, power density spectra of the entire outburst and specific observations. Total power spectrum reveals harmonics of the pulse which provides another method of verification to the pulse period. Later, the discovery of a marginal QPO in a single observation is discussed and presented. The pulse profiles acquired from the folded light-curve are also presented and the evolution of the morphology of these profiles are discussed. In accordance with the pulse profile evolution, time and flux resolved spectroscopy results are presented. These include a preliminary analysis where a blackbody model is tested. Conclusive spectral analysis is performed with the partially covering fraction absorption as its statistically preferable and provides better results in the low flux observations.

The physical explanations of all the results are discussed in Chapter 3. These include a review of the past studies of 2S 1417-624 in both this 2018 giant outburst and previous outbursts. The acquired results are first compared with previous studies and similar sources. Afterwards, the results are discussed in term of theoretical models. This thesis in the end aims to provide a larger picture regarding how outbursts effect X-ray binaries.

CHAPTER 2

ANALYSIS AND RESULTS

This chapter consists of the observational part of this thesis. It first describes the data selection methodology and then how to calibration and filtering methods Afterwards, it briefly delineates to the timing and spectral analysis procedures. Finally the resulting material that came out after the analysis process is being presented. Throughout the chapter, entirety of the data reduction process and analysis are done by using *HEASoft 6.28*[1]. The specific names of the tools or software that is a part of HEASoft FTOOLS family will be mentioned in the following sections. It should also be noted that all the results presented in this thesis were used while preparing the publication Serim et al. (2022)[38].

2.1 Observation Selection

This thesis utilizes of *NICER*/XTI ToO observations of 2S 1417-624 during its 2018 giant outburst. Upon those 86 observations, those with exposure times higher than 250s were taken into account because observations with lower exposure time would yield insufficient count rates for spectral modeling. These remaining 60 observations were acquired from HEASARC archive NICER Master Catalogue and are publicly accessible[2]. The list of observations that were used for timing and spectral analysis of this thesis could be found in figure 2.1. The outburst event in question is started to be observed by *NICER* at April 1st and ended at September 3rd 2018. During this five months of monitoring, 2S 1417-624 first exhibits an increase in flux and then once the peak is reached, a gradual decay takes place.

[1] `https://heasarc.gsfc.nasa.gov/docs/software/lheasoft/`
[2] `lhttps://heasarc.gsfc.nasa.gov/W3Browse/nicer/nicermastr.html`

Table 2.1: NICER TOO Observations that were used in this thesis

OBSID	Time (MJD)	Exposure (s)	OBSID	Time (MJD)	Exposure (s)
1200130101	58209.5141	443	1200130145	58276.00903	1048
1200130104	58214.48978	686	1200130146	58278.64757	903
1200130106	58219.37892	199	1200130147	58279.03402	448
1200130107	58221.9985	592	1200130148	58280.06389	1419
1200130108	58223.0285	1063	1200130149	58282.18744	429.1
1200130110	58225.02429	268	1200130150	58283.99421	468
1200130114	58233.1213	3938	1200130151	58289.0585	1133
1200130115	58236.33884	1433	1200130152	58290.6658	642
1200130116	58237.56108	1274	1200130153	58292.08449	1294
1200130117	58238.07425	1688	1200130154	58293.75394	164
1200130118	58239.29765	2029	1200130155	58296.13416	1591
1200130119	58240.79368	1042	1200130156	58297.42094	1598
1200130120	58241.22477	3470	1200130157	58298.45009	834
1200130122	58244.12056	1222	1200130160	58301.47424	595
1200130123	58245.08449	1109	1200130165	58308.23704	1294
1200130124	58246.04931	3380	1200130166	58310.18495	639
1200130126	58248.10928	3558	1200130167	58311.3328	900
1200130127	58249.92428	178	1200130168	58312.42543	872
1200130128	58250.05275	1302	1200130169	58317.55667	371
1200130129	58251.14926	2502	1200130171	58321.54838	480
1200130130	58252.0525	539	1200130172	58322.76664	307
1200130133	58260.0044	1475	1200130173	58323.67639	420
1200130134	58261.16432	330	1200130174	58324.63527	595
1200130135	58262.0722	622	1200130175	58326.1172	1321
1200130139	58269.37986	909	1200130177	58328.82294	574
1200130140	58271.18264	1593	1200130181	58338.77417	1509
1200130141	58272.53469	2632	1200130184	58354.34348	1147
1200130142	58273.37093	517	1200130185	58364.75326	354
1200130143	58274.33595	984	1200130184	58354.34348	1147
1200130144	58275.04398	806	1200130185	58364.75326	354

2.2 Data Reduction

The selected data are held subject to a data reduction through a data reduction process where the observations are filtered from external effects such as Earth-bound noise, interstellar flares and instrumental malfunction. In order to apply necessary calibration and filtering to the NICER observations used in this thesis, the data filtering tool of *NICER NICERDAS* is used. This tool is also a part of the greater HEASoft software family and in this thesis, NICERDAS version 7a is used. NICERDAS consists of several different commands and one one multitasking tool, `nicerl2`, that performs several data screening procedures at once and provides a calibrated level 2 data. This "level 2 calibration" provides a "standard processing" of the NICER data through series of scripts called *pipeline* and consequently the data the data is calibrated with nicercal, filtered *niprefilter* and *nimaketime)* merged and screened (`nimpumerge`. More details about data reduction commands of NICERDAS `nicerl2` can be found on its guide[3]. `nicerl2` provides options to be specified during the overall screening operation; however, we proceed with the default options that are recommended by NICER team[33]. These default recommended parameters provides the exclusion of the data when :

- the pointing offset is greater than $0.015°$
- the instrument goes through South Atlantic Anomaly.
- the bright Earth limb is greater than $30°$
- the dark Earth limb is greater than $15°$

In order to apply data calibration, the NICER XTI calibration files published by the NICER team with the version "CALDB 20200202" are used[4]. After all the observations are being put into nicerl2 data processing, resulting files, most importantly clean event files are then put into different processes according to the needs of the type of the further analysis. The timing and spectral data requires different preparations and they will be mentioned in their corresponding sections.

[3] https://heasarc.gsfc.nasa.gov/lheasoft/ftools/headas/nicerl2.html
[4] https://heasarc.gsfc.nasa.gov/docs/heasarc/caldb/data/nicer/xti/index/cif_nicer_xti_20200202.html

Finally, it should be noted that this overall calibration and cleaning process is mutually shared with the paper published with the analysis material of this thesis, Serim et al. (2022)[38].

2.3 Timing Analysis

In order to conduct the timing analysis, the light curves are generated from the cleaned events by using *XSELECT* tool within HEASoft package mentioned in the introductory paragraph of Chapter 2. During the light curve extraction process, Pulse Invariant(PI) is constraint with the nominal operating range of NICER using 30-1200 channel range with the time resolution 0.125s. The generated light curves are then put into a barycentric correction process where photon arrival times are adjusted according to the motion of the telescope such that the photon arrival takes place at the sun instead of an orbit of the telescope. This correction is done via *barycorr* tool of HEASoft. All the generated light curves are barycentrically corrected by making use of the orbit files of each event which are based upon the ephemeris DE430 of Jet Propulsion Laboratory.

2.3.1 Total Light Curve

The generated light curves of all the observations are first plotted in order to see the overall flux evolution of the giant outburst. The total light curve can be seen in Figure 2.1. It shows a rapid increase in flux immediately in the early stages of the giant outburst. Once it reaches the peak of the outburst, then a steady decrease in flux occurs where the source reaches nominal values in a matter of 6 months.

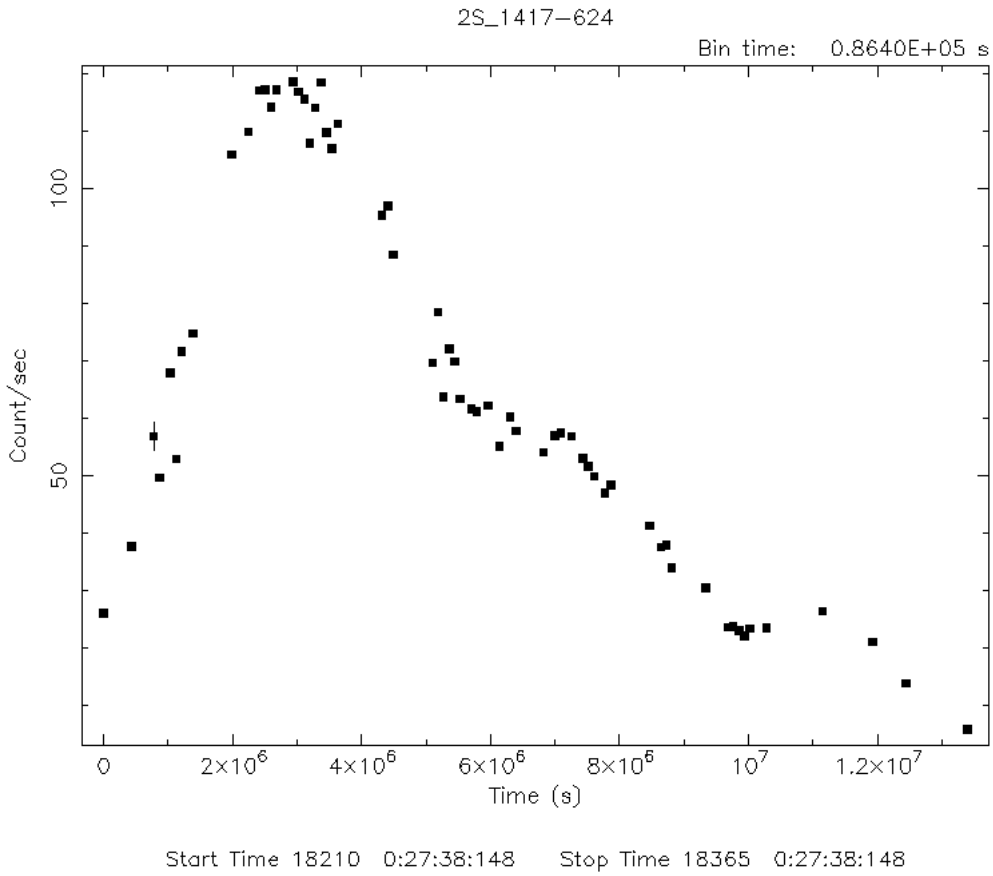

Figure 2.1: Total Light Curve of 2S 1417-624 During its 2018 giant outburst created via *NICER* ToO observations. The light curve is binned with bin time 86400s(1 day) by using lcurve. Observations that yielded problematic and unusual light curves were extracted.

2.3.2 Power Spectrum

Power spectrum of the source is generated and investigated by making use of *Powspec* tool of HEASoft. Firstly, the power spectrum of the combined light curve is investigated in order to acquire the to understand overall shape of the continuum of the power spectrum and pulse signals. This power spectrum of the combined light curve which spans the entire outburst can be found in Figure 1.14 This power spectrum shows very strong pulse signal with harmonics up to 9th degree. Frequency differences between each of those harmonics are almost equal and yield the spin period of the BeXRB. This average difference between the pulse and each harmonic is around

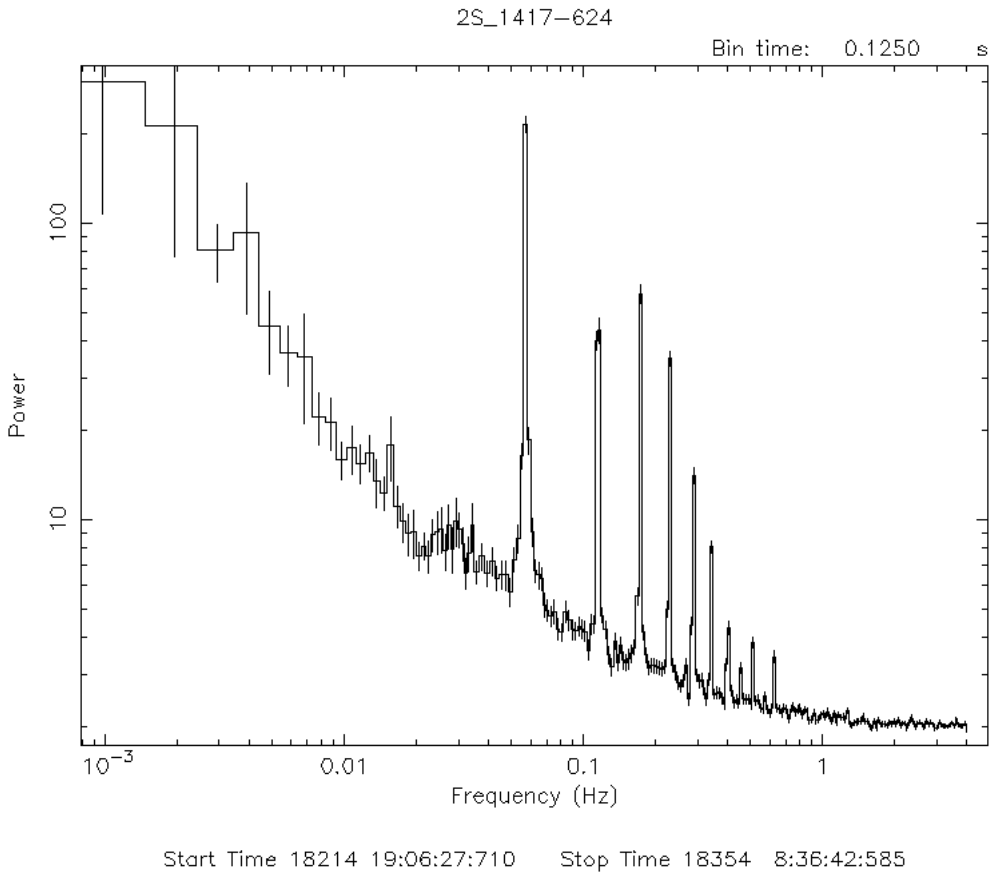

Figure 2.2: Power spectrum of 2S 1417-624 generated from the combined NICER light curves of the whole 2018 outburst. This power spectrum uses default 8192 bins with 0.125 s rebinning and the power spectrum is also geometrically rebinned with an order of -1.02 for visualization purposes.

0.57 Hz which is 17.4 s. This measurement is consistent with the folded light curve periodicity searches in Section 2.3.3. It will later be discussed in the next chapter that these spin period measurements via timing analysis are consistent both with past studies and FERMI/LAT observations.

2.3.2.1 Marginal QPO

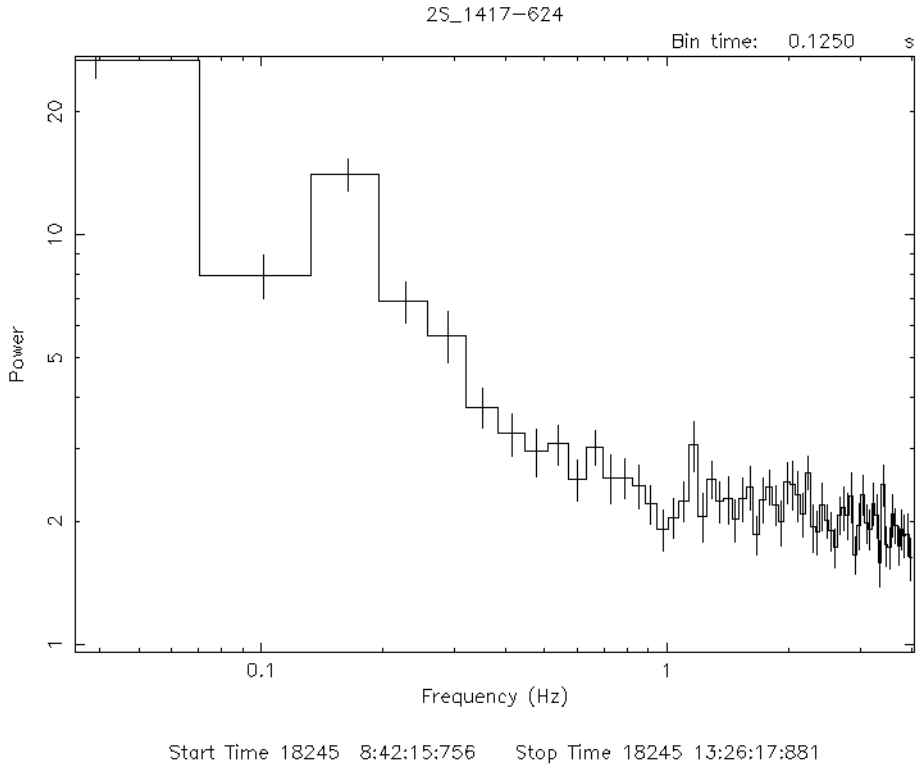

Figure 2.3: Power spectrum of Obs. ID. "1200130123"

After the power spectrum of the combined total light curve is investigated, the power spectra of each observation was generated individually and variations were examined for any excess signals or irregularities in the pulsations. Upon these individual power spectra, a small but unusual marginal "bump" was observed around 1 Hz in the observations some time after the outburst. This marginal QPO is best observed in the power spectrum taken on MJD 58245 which can be seen in Figure 2.3. This power spectrum is taken from an observation after the outburst. In order to better demonstrate the evolution of the marginal QPO, a power spectrum which shows no sign of such marginal QPO is also presented in Figure 2.4. This power spectrum is taken from an observation taken on MJD 58248, sometime after the observation that yielded the strongest marginal QPO structure, implying that this structure is short lived and rapidly diminished after its existence. Both power spectra presented in this thesis, alongside with many others in each NICER light curve provided from the observations in 2.1 are generated with 512 bins and 0.125 rebinning time. This created a splitting of the light

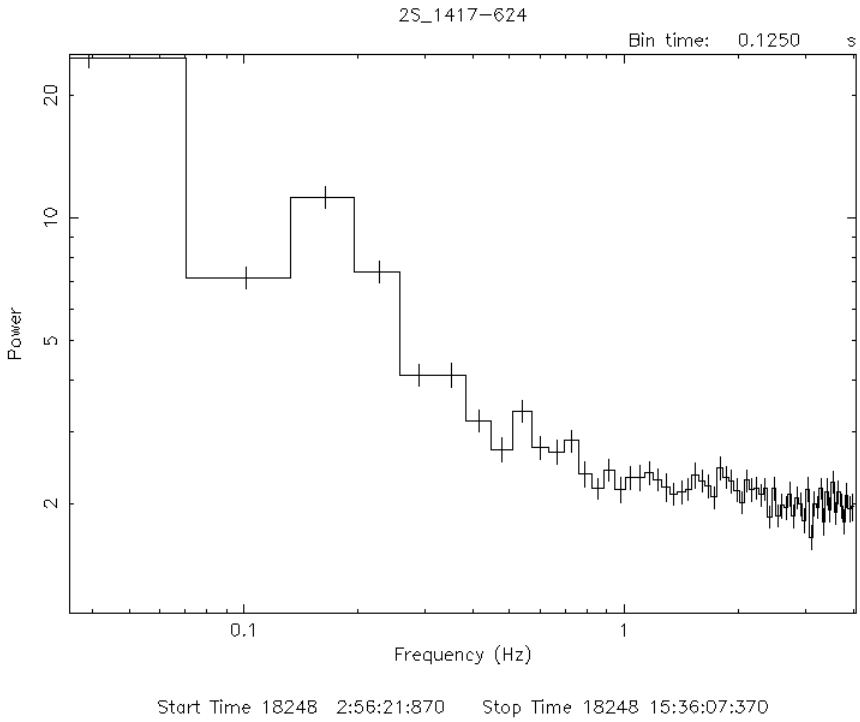

Figure 2.4: Power spectrum of ID. "1200130126"

curve into 64 s time intervals which is then averaged into a single frame. This power spectrum with the same configuration can also be found in the paper published from this thesis[38].

After this suspected marginal QPO is searched throughout the entire outburst, it is understood that the power spectrum at Figure 2.3 provides the strongest signal. In order to acquire this, firstly first two data points which are insignificant for investigating the marginal QPO is excluded from the power spectrum. Afterwards, the remaining data was fitted by using a smooth broken power law1.1.5.2 to describe the continuum and with Lorentzian1.1.5.4 to describe the QPO structure. Furthermore, this power spectrum is then divided into the continuum model and the power is multiplied by two in order to achieve the corresponding σ levels. The resulting analysis is shown in Figure 2.5 which taken from the publication that yielded as a result of this thesis, Serim et al. 2022[38].

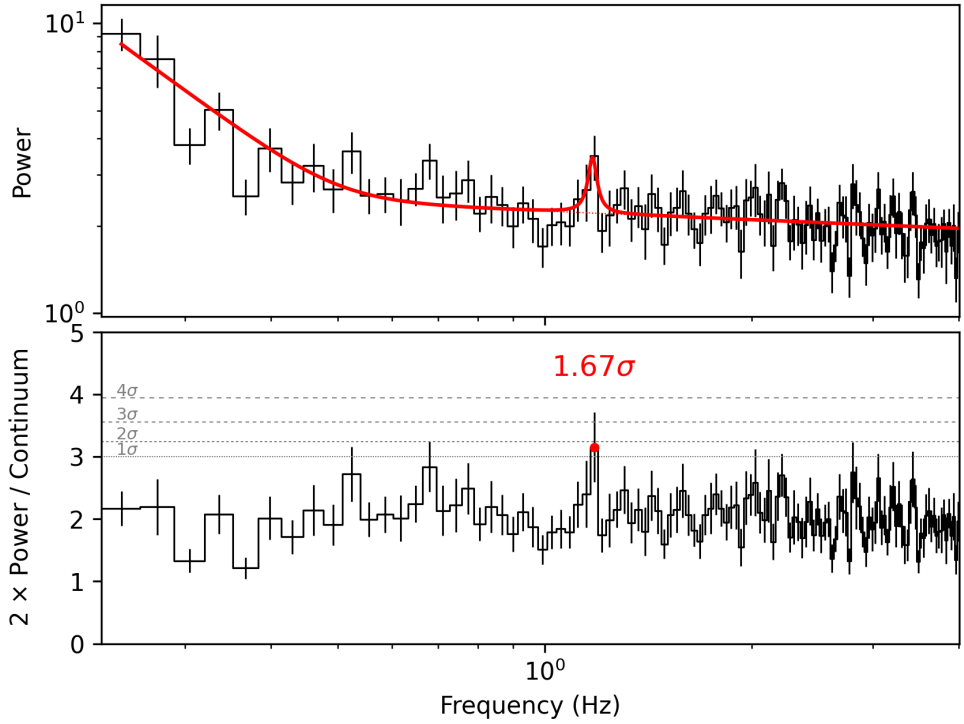

Figure 2.5: Upper Panel: Power spectrum where the strongest feature of the marginal QPO is shown. The line shows the model continuum which, alongside with the analytical details of the power spectrum is described in the main text of this section. Lower Panel: A sigma test that was applied to this continuum in the upper panel. The peak of the marginal QPO shows a deviation from the continuum with the significance level of 1.67σ.

2.3.3 Spin Period Measurements

It is previously pointed out by *Fermi*/LAT that rapid monitoring of the yields around 17.4 s of spin period during the time of the observations[5]. This result is further verified by investigating the folded light curve by *efsearch* tool of HEASoft. The resulting analysis can be found in Figure 2.3.3.

[5] https://gammaray.nsstc.nasa.gov/gbm/science/pulsars/lightcurves/2s1417.html

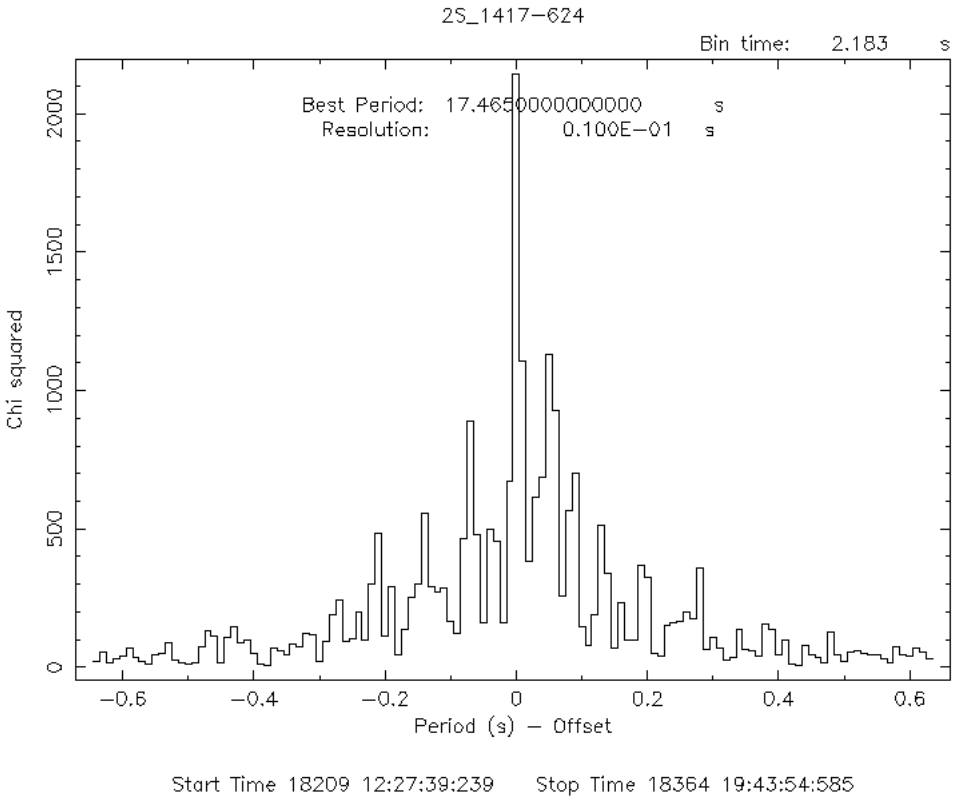

Figure 2.6: The spin period search result of 2S1417-624. The central peak at the origin clearly shows the best period at 17.465 with a resolution of 0.01.

2.3.4 Pulse Profiles

When the effects of the outburst is firstly observed at the total light curve, the next step was to investigate how does the pulse shapes vary by creating folded light curve figures before, during and after the outburst with an aim of understanding the luminosity dependent nature of the pulse profiles reported by [23]. These figures can be seen at: Figures 2.7, 2.8 and 2.9.

In the lower flux regions, pulse profile tends to show a single peak property with a small local maxima after the large peak. It can later be seen that as the consequence of the outburst, the system evolves into a double and even triple peak behavior. This occurrence is directly related to the rapid change in the accretion regime as flux increases and decreases. This flux dependent change in the accretion geometry is further discussed in the next chapter. In order to better and more precisely comprehend the

consequences of and determine the possible reasons laying behind why this change in the accretion regime occurs, spectral properties of the source is investigated.

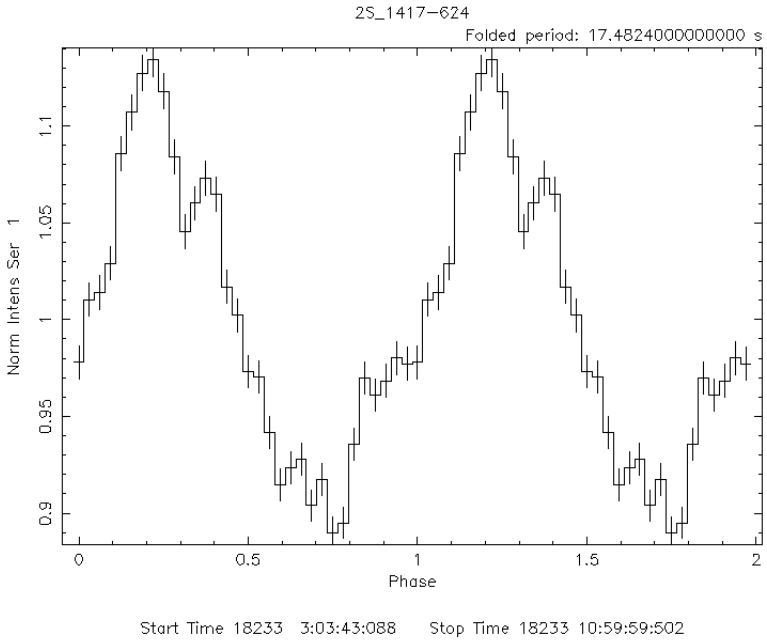

Figure 2.7: Pulse profile of 2S 1417-624 just before the outburst

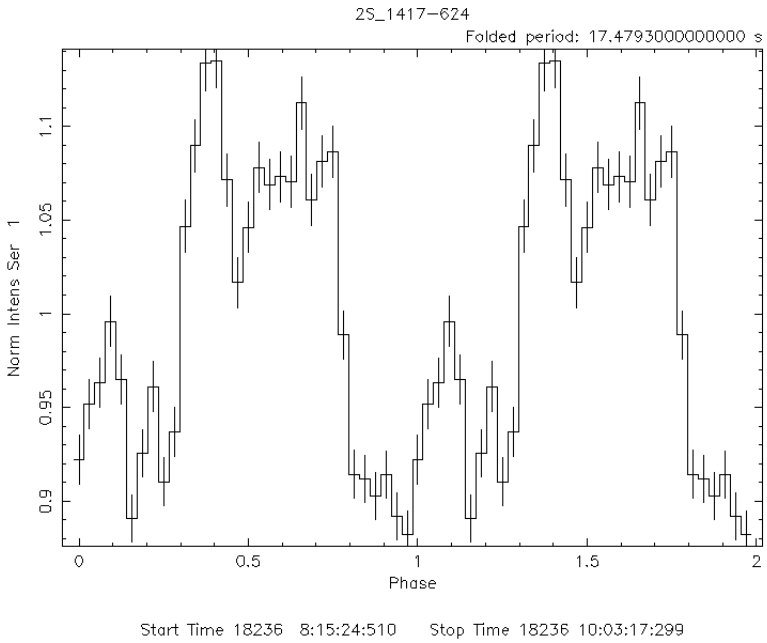

Figure 2.8: Pulse profile of 2S 1417-624 right at the peak of the outburst

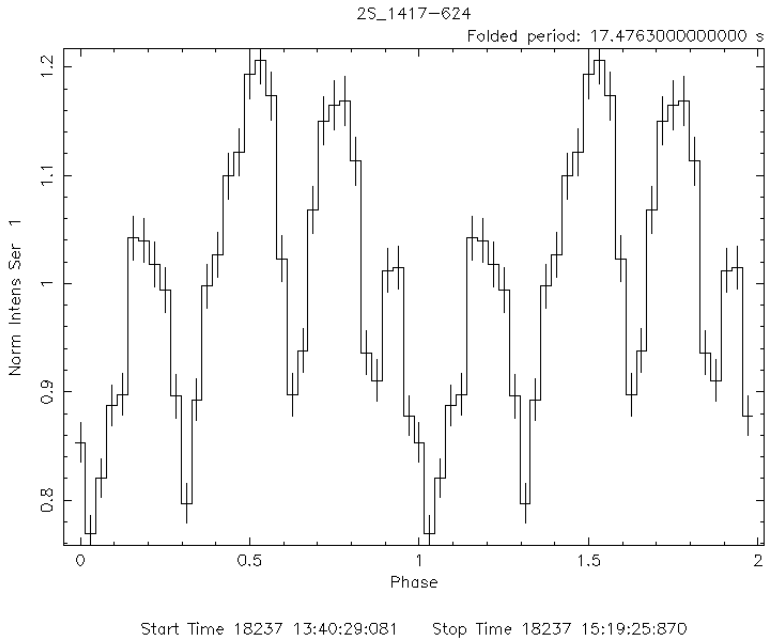

Figure 2.9: Pulse profile of 2S 1417-624 right after the outburst

2.4 Spectral Analysis

In order to conduct the spectral analysis, the cleaned and calibrated events generated in Section 2.2 are used to extract the spectra of individual observations. This extraction process is done via a background estimator tool.

2.4.1 Background Reduction and Calibration

2S 1417-624 is a galactic source and contribution from external sources interfering with the observational data is highly likely. Therefore it is vital for conducting spectral analysis to reduce these external contributions from to be analyzed spectra. In order to achieve this goal, the *NICER* team has recommended using two background models to be used for such purpose[6]. Upon these background estimator tools, *nibackgen3C50*[37] subtracts the X-ray background data from all sky catalogue of 3C50 background libraries and generates good-time intervals(GTI) according to the interference close to NICER detectors. The background and total spectra are generated

[6] `https://heasarc.gsfc.nasa.gov/docs/nicer/tools/nicer_bkg_est_tools.html`

by nibackgen3C50 and used in the further analysis. This further analysis is done by XSPEC tool version 12.11.0 that is a part of HEASoft. The response files necessary for the spectral analysis are provided by the NICER team.[7] The used versions for these response files are; "20170601v004" for the ancilliary response file(ARF) and "20170601v002" for the redistribution matrix file(RMF). However, upon these response files, two NICER detectors among the fifty six ones(number 14 and 34) are excluded in accordance with the recommendations of the NICER team.[8] The produced total spectra are then gone through a rebinning process by using `grppha` tool of HEASoft where each bin shall have at least 30 counts. Finally the energy range of 0.8-12.0 keV is taken into account both because NICER team recognizes as "low energy noise"[9] flares below 0.5 keV. Additionally, the background model used and the spectra failed to match below 0.8 keV. The harder energy range of the NICER spectra on the other hand turned out to be less problematic.

2.4.2 Model Selection

The generated spectra is then put into several models with the accordance of the theoretical explanations of BeXRBs. It is almost certain for high energy sources like 2S 1417-624 to show power law features. It has been previously observed by İnam et al. (2004) that the power law component in this source also shows a significant high energy cutoff[21]. Additionally, since the emitted light from pulsars reflects Iron from the temporary accretion disk, it is also expected to observe Iron line emission features in the spectrum. When these contributions are added and analysis has been conducted, it was seen that further model contributions might also be required to explain the physical properties of the source. One of these candidate models would be the contribution of a blackbody since pulsars at BeXRBs contain hot spots on the magnetic polar caps and some thermal emission is observed and explained by the blackbody model. Therefore, one of the model combinations to be chosen for the analysis at each spectra was a power law with a high-energy cutoff, a Gaussian

[7] https://heasarc.gsfc.nasa.gov/docs/heasarc/caldb/data/nicer/xti/index.html

[8] https://heasarc.gsfc.nasa.gov/docs/nicer/data_analysis/nicer_analysis_tips.html

[9] https://heasarc.gsfc.nasa.gov/docs/nicer/data_analysis/nicer_analysis_tips.html

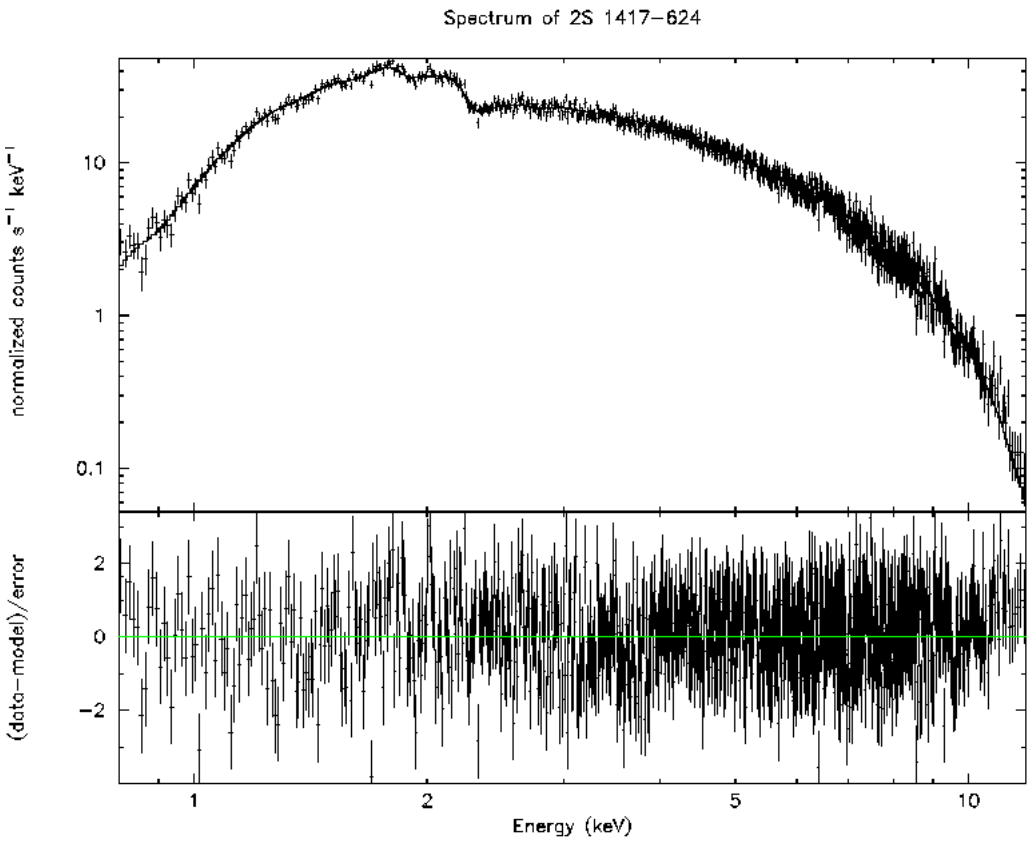

Figure 2.10: An example spectrum of 2S 1417-624 fitted with the model configuration involving partial covering fraction absorption. OBSID: 120130123

Iron fleurescent line and finally a blackbody. An additional model combination was later selected after the expected results has not been achieved from the blackbody model. This combination suggests the existence of a material partially covering the pulsar. This model configuration that was chosen to conduct a spectral evolution study consists a partial covering absorber instead of blackbody in the previously defined model combination. A partial covering absorber model was also previously suggested for 2S 1417-624 by Gupta et al. (2019)[16].

2.4.3 Spectral Evolution

The spectral analysis in this thesis is done almost entirely by applying chosen model fits to each spectra throughout the observation of the giant outburst. This spectral evolution is then used to determine any variations in the spectral parameters due to time and/or flux.

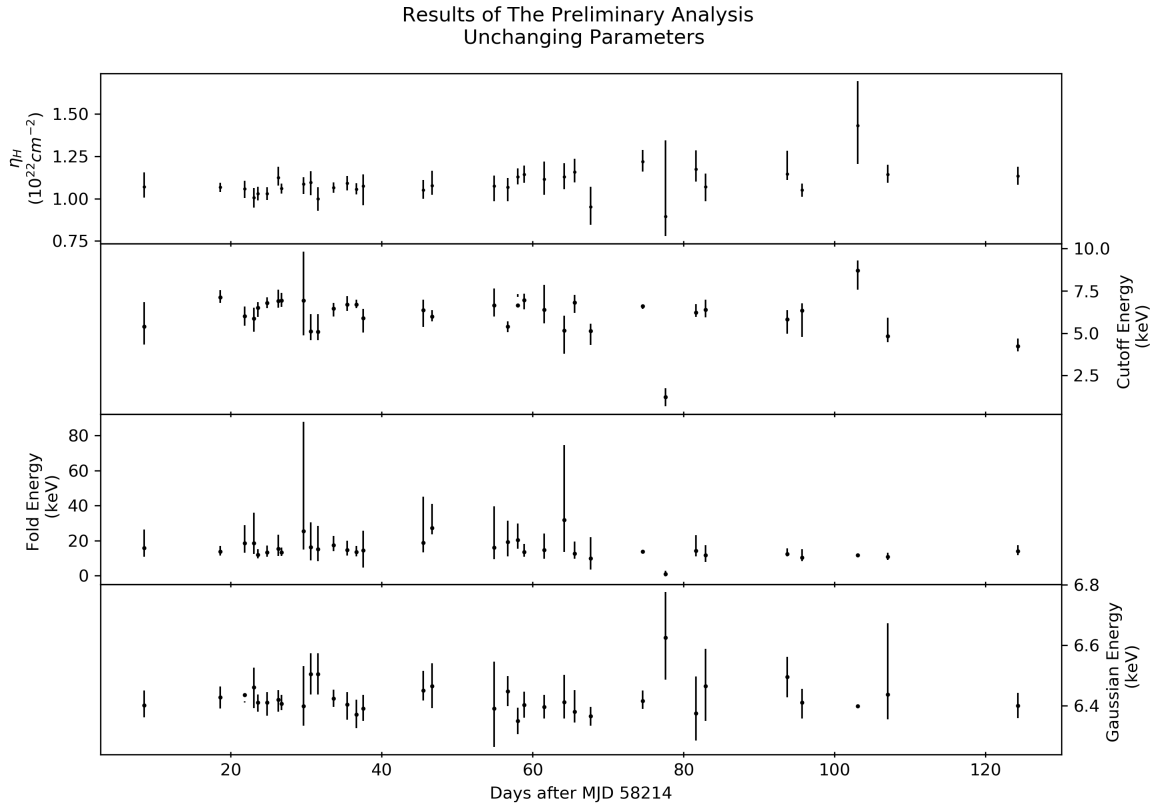

Figure 2.11: Results of the preliminary spectral evolution where parameters shown provide little to no variation.

2.4.3.1 Preliminary Analysis

Firstly, a preliminary analysis where all the parameters of the applied spectral models were set free in each individual spectra. This provided the result that High-Energy cutoff and Gaussian Iron line parameters remain almost constant and show no significant variation throughout the outburst. Likewise Iron line width and sigma shows little to no change as well. This result can be seen in Figure 2.11.

This realization pushed for a further analysis of the spectral evolution with these unchanging model parameters or parameter values beyond the 0.8-12 keV energy window to be fixed. With that, the parameter values are fixed into following values:

- Cutoff Energy to 8.09 keV
- Fold Energy to 13.91 keV
- Gaussian Energy to 6.44 keV. That is the already existing Fe Kα line observed in laboratories.
- Gaussian Sigma to 0.001 for convenience and for the Gaussian model not to dominate the entire spectrum in faint observations where Iron line is not visible enough.
- Hydrogen Column parameter of the Photon Absorption model also remains unchanged, at the values very close to the Galactic X-ray background average.[10]

Likewise, when the entirety of the spectra is applied a blackbody addition to the existing models, statistically insignificant results were achieved especially as the flux of the observations reaches to lower values past the peak of the outburst. It should also be reported that the fitting process was particularly slow to the point that it was challenging for XSPEC to fit the spectral parameters of the blackbody into a reasonable value which resulted very high errors in some data points. When checked, these observations did not turn out to be problematic, implying the cause of the problem may be that as the flux diminishes, blackbody component becomes statistically insignificant. This can be seen in Figure 2.12 where some correlation due to flux can

[10] `https://heasarc.gsfc.nasa.gov/cgi-bin/Tools/xraybg/xraybg.pl`

be observed for a while during the peak of the outburst but in some cases kT values reaches to unreasonable values (e.g. ~ 3 keV) and radius of the blackboddy emitting region drastically leaps. Further discussion on the reason of this phenomenon will be made in the following chapter.

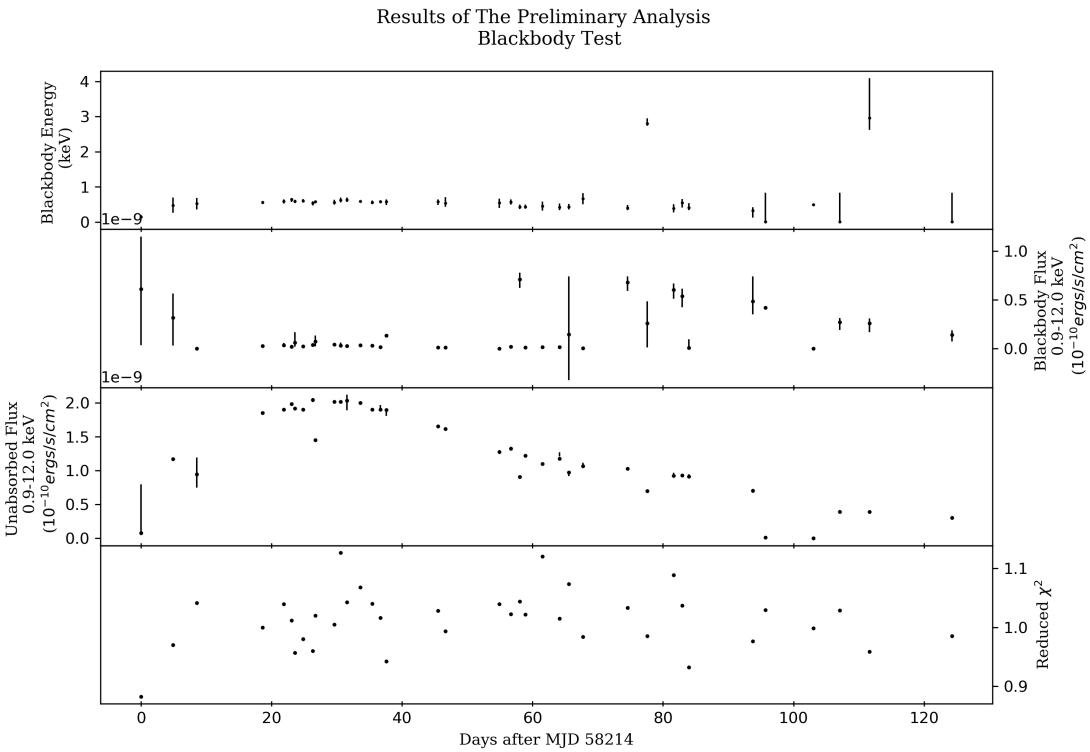

Figure 2.12: Resulting spectral evolution of the preliminary analysis with Blackbody model.

2.4.3.2 Consequent Analysis

The resulting figure 2.12 of the blackbody model impelled the study further into making research about new models and physical explanations. As a consequence of this further research, as mentioned in Section 2.4.2, a partially covering material is placed into the analysis and the Blackbody was excluded. This yielded more reliable and convenient parameter variations which are shown in Figure 2.13 that allowed further physical discussion to be made. This physical discussion will be elaborated further in the next chapter.

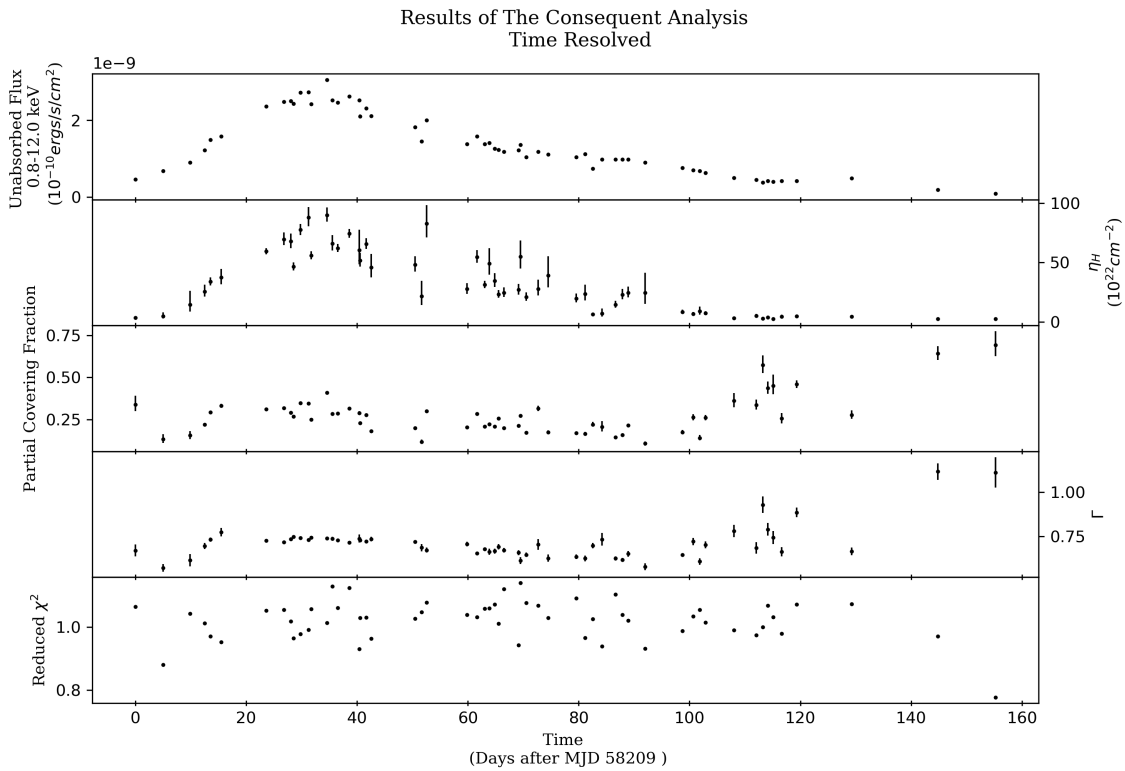

Figure 2.13: Time resolved spectroscopy of 2S 1417-624 with PCAF model applied alongside with previous configurations where as an addition, parameters that show no change are fixed.

Time Resolved Spectroscopy It is possible to observe in Figure 2.13 that the Hydrogen Column(η_H) of PCAF is perfectly aligned and correlated with the flux and there is a direct correlation between the Partial Covering Fraction of PCAF and the Spectral Index(Γ) of the power law. All the parameters show some degree of increase as the giant outburst progresses. However, past the 100 days since the start of the observations, a rapid increase that suppresses the degree of increase at the peak of the outburst can be seen in Γ alongside with Partial Covering Fraction. This implies a luminosity dependent spectral behavior as the folded light-curve analysis also yielded which will be explained further in the next chapter.

Flux Resolved Spectroscopy Considering the revealed relationship of the model parameters with the flux, an analysis of the evolution of spectral parameters was in order, for investigating the nature of this change in accretion even further. The resulting

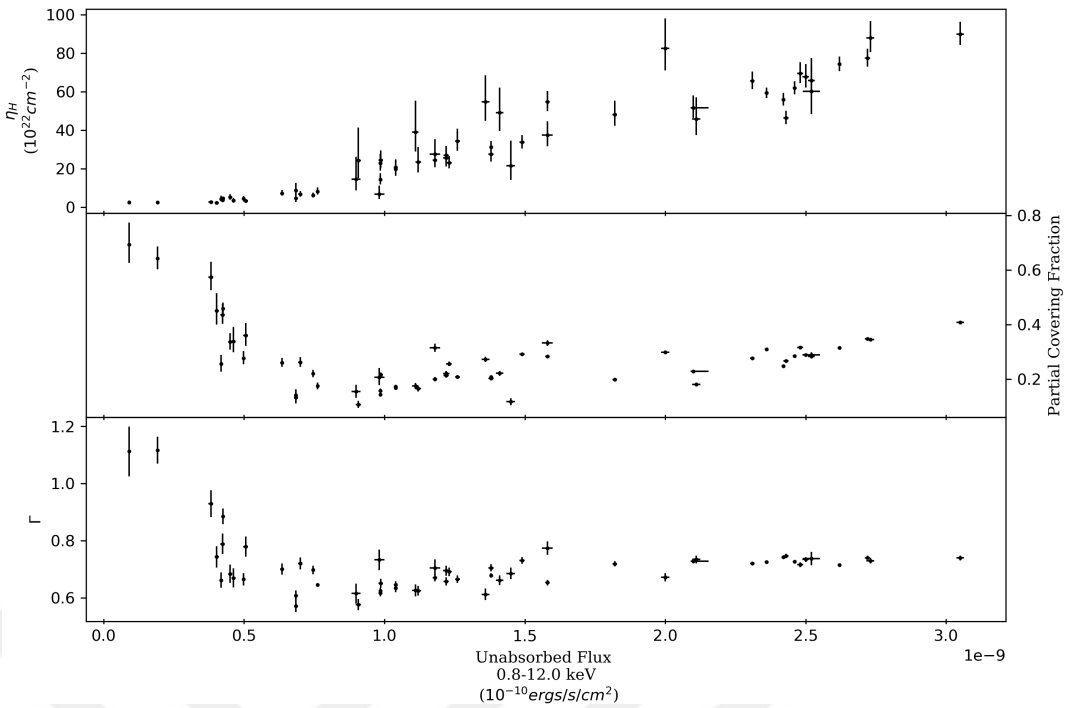

Figure 2.14: Flux resolved spectroscopy of 2S 1417-624 with PCAF model applied alongside with previous configurations where as an addition, parameters that show no change are fixed.

Figure 2.14 provides a clearer setup for better understanding how flux or luminosity effects the spectral parameters.

The Figure 2.14 clearly shows a direct correlation with η_H and flux after passing the low flux region. Γ and Partial Covering Fraction on the other hand starts high and provides a rapid decrease after which they too start steadily to be correlated with the flux. This flux level that triggers a change in the correlation should be the critical luminosity level where the accretion regime changes. The nature of such a behaviour will be discussed in the next chapter.

CHAPTER 3

DISCUSSION AND CONCLUSION

This thesis focuses on the particular giant outburst that took place at the BeXRB 2S 1417-624 in 2018 and aimed to produce several conclusions amongst such types of sources by making use of the spectral and timing analysis results which were generated from *NICER* ToO observations of the outburst. In order to achieve this goal in this chapter, firstly the results of this thesis were discussed and compared with the previous studies of 2S 1417-624. Afterwards, these results were compared with the results of other studies on other BeXRBs. It was aimed by this methodology that the effects and causes of the outbursts on such transient sources might physically be better explained.

When the overall *NICER* light-curve of the source was examined; the structure, shape and the behaviour of the flux turned out to be quite consistent with FERMI-LAT[1], Swift/BAT[2], NuStar[16] and Insight/HXMT[23] light-curves, produced during this outburst. The light-curves of this 2018 giant outburst also showed similar properties and profile with the previous outbursts. This situation made it possible consider that such giant outbursts regularly occur on 2S 1417-624 and it is plausible to predict an occurrence of a giant outburst in this source in the future years to come.

In the case of the power-density spectrum and the marginal QPO, it has been a very common experience to report QPO-like structures or even investigate the power spectrum. It is known for HMXRBs to show little-to-no accretion disk to provide. However, in BeXRBs, transient temporary accretion disks are observed. The most common explanation for the QPOs observed in the X-ray binaries is the non-homogenity

[1] `https://gammaray.nsstc.nasa.gov/gbm/science/pulsars/lightcurves/2s1417.html`

[2] https://swift.gsfc.nasa.gov/results/transients/weak/H1417-624/

in the innermost parts of the accretion disk. Likewise, 2S 1417-624 is believed to acquire some temporary accretion disk during its periastron passage. One example for such an observed QPO in a BeXRB system would be GX 304-1 where a QPO is observed around 0.125Hz and at a similar time of its corresponding outburst in 2010[11]. However, this QPO in GX 304-1 was visible for 12 days and provided a harmonic. The marginal QPO found at 2S 1417-624 during its 2018 giant outburst on the other hand does not provide results significant enough to fully claim its existence. This prevents this thesis to focus further into this discussion.

When the folded light curve is investigated, the pulse profile searches turn out to be consistent with the previous studies on 2S 1417-624 during its 2018 giant outburst where both of these previous studies also determined the period to be around 17.47[16][23].

The nature of the pulse profiles of 2S 1417-624 is dynamic and underwent an evolution in its profile from a single peak to a double peak and further even triple peaks with two major and one minor. This structural evolution signified a change in the accretion geometry and the generation of a double peak structure signals a mixture of different types of beams creating the accretion. This change interpreted as a phase transition which was triggered by the increasing luminosity reaching to the point of the critical luminosity[6] where beyond this value, radiative shocks occur and are sent to the accretion column. Existence of this situation in 2S 1417-624 is also encountered in 2018 by both the previous studies[16] and this thesis and in the earlier outbursts[21] as well. Example pulse profiles from literature were presented can be seen at Figure 3.1 taken from Gupta et al. (2019)[16]. The pulse profiles were obtained after the peak of the outburst and therefore a formation of the double peak structure from the single peak was complete. This indicated that the accretion geometry is altered to fan beam at the luminosities beyond the critical level and temporary accretion disk is also fed by the shock generated by the beam at the magnetic pole of the pulsar at high accretion rates. This certainly provided spectral features and that was the main reasoning of this thesis to investigate the spectra of the source.

It has been seen in the preliminary analysis that Blackbody model did not provide statistically significant results as flux decreases. Considering the fact that the ob-

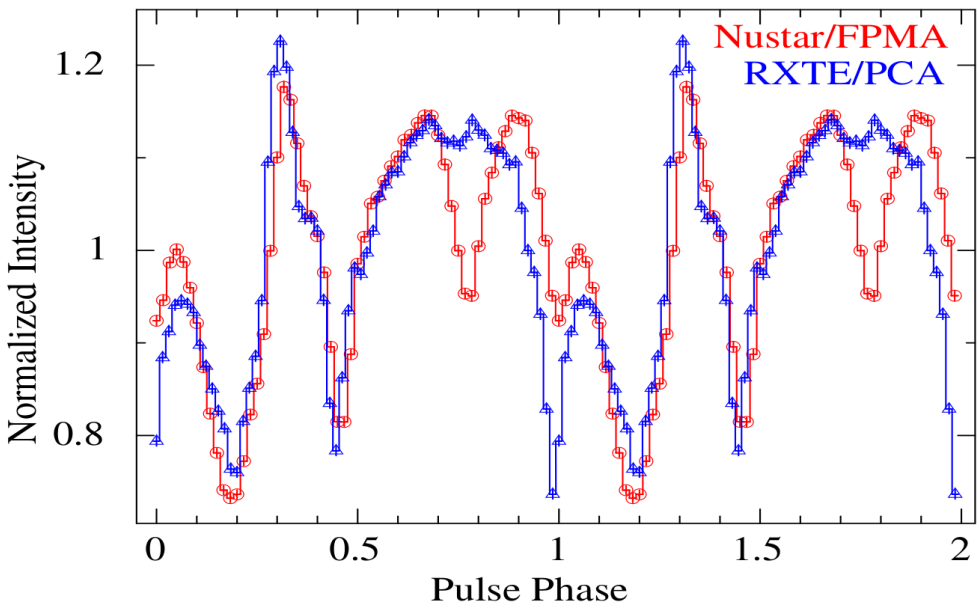

Figure 3.1: Pulse profiles of 2S 1417-624 generated with NuStar(Red) and RXTE(blue) observations after the peak of the outburst where a double peak structure beyond the critical luminosity is visible. This figure is directly taken fromfrom Gupta et al. (2019)[16]; Figure 2

servations were well able to provide statistically meaningful results in other model configurations provide two different scenarios. Either flux was not enough to resolve blackbody component anymore or no blackbody emission exists at low luminosity levels in this source.

On the other hand, PCAF model provides statistically suitable model even in low flux observations, thus enables to trace the spectral evolution throughout the outburst , even in the lowest flux observations. Whit this model, η_H showed significant correlation with the flux and this relation yields significant physical explanations. One possible explanation was due to an increase in the absorption at the accretion regime past the critical luminosity. This view could be supported by the changing pulse profiles as they experience a rather significant dips in their profile at super-critical accretion regime[23]. Another explanation for this correlation might be due to an overall absorption happening at the surrounding region of the pulsar which is not phase dependent (e.g. a quasi-static shell or envelope around the NS).

The spectrum provided the upper bounds of the critical luminosity as they can be traced through correlation mode switching between Γ and the covering fraction with flux. Because correlation mode switch of covering fraction could be due to the change in the morphology of the accretion column due to the high flux rates. When the shock generated as a consequence of the supercritical luminosity, the accelerated electrons start to diminish. Due to this newly formed oppositely-pressurized situation which causes partial covering fraction to stay anti-correlated with the flux until the critical level is reached and then transform into a slight correlation. Likewise, the slope of the positive correlation of η_H increases after the critical level is reached, implying an accretion regime change due to the oppositely pressurised shock.

Similar flux-dependent behaviour of Γ were also observed during the previous giant outburst of 2S 1417-624 and it had then been explained due to the X-ray producing Comptonization occurs in a region between the surface of the neutron star and the generated shock. Once the shock was spread out as the critical luminosity levels were reached, then the anti-correlation turned slowly into a slight correlation. The shock affected the energy of the accelerated electrons to the level that the processes producing power-law and X-ray photon reduces, but once the shock has passed and the transition takes place, the source slowly start to increase producing inverse-Comptonization and therefore an increase in Γ is observed.

This observed critical region and luminosity value was also consistent with previous studies of this outburst[23] and provides further evidence for this accretion regime transition existing suspicion in the pulse profiles were verified by the spectral evolution. This change in the accretion regime was triggered by the increasing luminosity and as a consequence a generated radiation-dominated shock. This shock reaches to already pressurized accretion disk and complicates the accretion regime. This is clearly visible in the flux resolved spectral evolution.

In order for the results and discussions in this thesis to become more prevalent, future outbursts of this source must be studied. Additionally, phase dependent behaviour of the partial covering and Γ components should be investigated. A correlation between the dips at the pulse profiles and Γ could be seen which provides more clear explanations describing the nature of the pulse profile morphology and the accretion regime

transformation. Additionally, components which were not yielded parameter values within the energy window of *NICER* would be investigated by analyzing the observations of different instruments with different energy ranges. Finally, a multiwavelength analysis may also be conducted by observing the companion star in different wavebands.

REFERENCES

[1] K. M. V. Apparao, S. Naranan, R. L. Kelley, and H. V. Bradt. 2S 1417-624 : a variable galactic X-ray source near CG 312-1. , 89:249–250, Sept. 1980.

[2] G. B. Arfken, H. J. Weber, and F. E. Harris. Chapter 20 - integral transforms. In G. B. Arfken, H. J. Weber, and F. E. Harris, editors, *Mathematical Methods for Physicists (Seventh Edition)*, pages 963–1046. Academic Press, Boston, seventh edition edition, 2013.

[3] Z. Arzoumanian, K. C. Gendreau, C. L. Baker, T. Cazeau, P. Hestnes, J. W. Kellogg, S. J. Kenyon, R. P. Kozon, K.-C. Liu, S. S. Manthripragada, C. B. Markwardt, A. L. Mitchell, J. W. Mitchell, C. A. Monroe, T. Okajima, S. E. Pollard, D. F. Powers, B. J. Savadkin, L. B. Winternitz, P. T. Chen, M. R. Wright, R. Foster, G. Prigozhin, R. Remillard, and J. Doty. The neutron star interior composition explorer (NICER): mission definition. In T. Takahashi, J.-W. A. den Herder, and M. Bautz, editors, *Space Telescopes and Instrumentation 2014: Ultraviolet to Gamma Ray*, volume 9144, pages 579 – 587. International Society for Optics and Photonics, SPIE, 2014.

[4] C. A. L. Bailer-Jones, J. Rybizki, M. Fouesneau, G. Mantelet, and R. Andrae. Estimating Distance from Parallaxes. IV. Distances to 1.33 Billion Stars in Gaia Data Release 2. , 156(2):58, Aug. 2018.

[5] Y. Bar-Yam. Concepts: Power law.

[6] P. A. Becker, D. Klochkov, G. Schönherr, O. Nishimura, C. Ferrigno, I. Caballero, P. Kretschmar, M. T. Wolff, J. Wilms, and R. Staubert. Spectral formation in accreting X-ray pulsars: bimodal variation of the cyclotron energy with luminosity. , 544:A123, Aug. 2012.

[7] E. Beklen, M. H. Finger, and GBM Pulsar Project Team. 2S 1417-624 in Outburst. *The Astronomer's Telegram*, 2275:1, Oct. 2009.

[8] H. Bondi. On spherically symmetrical accretion. , 112:195, Jan. 1952.

[9] M. Camenzind. *Compact objects in astrophysics : white dwarfs, neutron stars, and black holes*. 2007.

[10] Z. A. M. C. P. R. Craig Markwardt, Keith Gendreau. The neutron star interior composition explorer mission guide background section.

[11] J. Devasia, M. James, B. Paul, and K. Indulekha. Timing and spectral studies of the transient X-ray pulsar GX 304-1 during an outburst. , 417(1):348–358, Oct. 2011.

[12] K. Ebisawa, G. Bourban, A. Bodaghee, N. Mowlavi, and T. J. L. Courvoisier. High-energy sources before INTEGRAL. INTEGRAL reference catalog. , 411:L59–L62, Nov. 2003.

[13] K. C. Gendreau, Z. Arzoumanian, P. W. Adkins, C. L. Albert, J. F. Anders, A. T. Aylward, C. L. Baker, E. R. Balsamo, W. A. Bamford, S. S. Benegalrao, D. L. Berry, S. Bhalwani, J. K. Black, C. Blaurock, G. M. Bronke, G. L. Brown, J. G. Budinoff, J. D. Cantwell, T. Cazeau, P. T. Chen, T. G. Clement, A. T. Colangelo, J. S. Coleman, J. D. Coopersmith, W. E. Dehaven, J. P. Doty, M. D. Egan, T. Enoto, T. W. Fan, D. M. Ferro, R. Foster, N. M. Galassi, L. D. Gallo, C. M. Green, D. Grosh, K. Q. Ha, M. A. Hasouneh, K. B. Heefner, P. Hestnes, L. J. Hoge, T. M. Jacobs, J. L. Jørgensen, M. A. Kaiser, J. W. Kellogg, S. J. Kenyon, R. G. Koenecke, R. P. Kozon, B. LaMarr, M. D. Lambertson, A. M. Larson, S. Lentine, J. H. Lewis, M. G. Lilly, K. A. Liu, A. Malonis, S. S. Manthripragada, C. B. Markwardt, B. D. Matonak, I. E. Mcginnis, R. L. Miller, A. L. Mitchell, J. W. Mitchell, J. S. Mohammed, C. A. Monroe, K. M. Montt de Garcia, P. D. Mulé, L. T. Nagao, S. N. Ngo, E. D. Norris, D. A. Norwood, J. Novotka, T. Okajima, L. G. Olsen, C. O. Onyeachu, H. Y. Orosco, J. R. Peterson, K. N. Pevear, K. K. Pham, S. E. Pollard, J. S. Pope, D. F. Powers, C. E. Powers, S. R. Price, G. Y. Prigozhin, J. B. Ramirez, W. J. Reid, R. A. Remillard, E. M. Rogstad, G. P. Rosecrans, J. N. Rowe, J. A. Sager, C. A. Sanders, B. Savadkin, M. R. Saylor, A. F. Schaeffer, N. S. Schweiss, S. R. Semper, P. J. Serlemitsos, L. V. Shackelford, Y. Soong, J. Struebel, M. L. Vezie, J. S. Villasenor, L. B. Winternitz, G. I. Wofford, M. R. Wright, M. Y. Yang, and W. H.

Yu. The Neutron star Interior Composition Explorer (NICER): design and development. In J.-W. A. den Herder, T. Takahashi, and M. Bautz, editors, *Space Telescopes and Instrumentation 2016: Ultraviolet to Gamma Ray*, volume 9905 of *Society of Photo-Optical Instrumentation Engineers (SPIE) Conference Series*, page 99051H, July 2016.

[14] P. Ghosh, F. K. Lamb, and C. J. Pethick. Accretion by rotating magnetic neutron stars. I. Flow of matter inside the magnetosphere and its implications for spin-up and spin-down of the star. , 217:578–596, Oct. 1977.

[15] J. E. Grindlay, L. D. Petro, and J. E. McClintock. Optical identification of 2S 1417-62. , 276:621–624, Jan. 1984.

[16] S. Gupta, S. Naik, and G. K. Jaisawal. NuSTAR view of Be/X-ray binary pulsar 2S 1417-624 during 2018 giant outburst. , 490(2):2458–2466, Dec. 2019.

[17] T. Güver and F. Özel. The relation between optical extinction and hydrogen column density in the Galaxy. *Monthly Notices of the Royal Astronomical Society*, 400(4):2050–2053, 12 2009.

[18] M. Hazra, S. Pal, M. Mandal, and B. Bhunia. Swift/MAXI/Fermi detection of strong X-ray activity from 2S 1417-624. *The Astronomer's Telegram*, 14349:1, Jan. 2021.

[19] A. Hewish, S. J. Bell, J. D. H. Pilkington, P. F. Scott, and R. A. Collins. Observation of a Rapidly Pulsating Radio Source. , 217(5130):709–713, Feb. 1968.

[20] S. Ç. İnam, A. Baykal, D. Matthew Scott, M. Finger, and J. Swank. X-ray flux related timing and spectral features of 2S 1417-62. , 349(1):173–180, Mar. 2004.

[21] S. Ç. İnam, A. Baykal, D. Matthew Scott, M. Finger, and J. Swank. X-ray flux related timing and spectral features of 2S 1417-62. , 349(1):173–180, Mar. 2004.

[22] F. Jankowski, W. van Straten, E. F. Keane, M. Bailes, E. D. Barr, S. Johnston, and M. Kerr. Spectral properties of 441 radio pulsars. *Monthly Notices of the Royal Astronomical Society*, 473(4):4436–4458, 10 2017.

[23] L. Ji, V. Doroshenko, A. Santangelo, C. Güngör, S. Zhang, L. Ducci, S. N. Zhang, M. Y. Ge, L. J. Qu, Y. P. Chen, Q. C. Bu, C. Cai, X. L. Cao, Z. Chang, G. Chen, L. Chen, T. X. Chen, Y. Chen, Y. B. Chen, W. Cui, W. W. Cui, J. K. Deng, Y. W. Dong, Y. Y. Du, M. X. Fu, G. H. Gao, H. Gao, M. Gao, Y. D. Gu, J. Guan, C. C. Guo, D. W. Han, Y. Huang, J. Huo, S. M. Jia, L. H. Jiang, W. C. Jiang, J. Jin, L. D. Kong, B. Li, C. K. Li, G. Li, M. S. Li, T. P. Li, W. Li, X. Li, X. B. Li, X. F. Li, Y. G. Li, Z. W. Li, X. H. Liang, J. Y. Liao, C. Z. Liu, G. Q. Liu, H. W. Liu, X. J. Liu, Y. N. Liu, B. Lu, F. J. Lu, X. F. Lu, Q. Luo, T. Luo, X. Ma, B. Meng, Y. Nang, J. Y. Nie, G. Ou, N. Sai, L. M. Song, X. Y. Song, L. Sun, Y. Tan, L. Tao, Y. L. Tuo, C. Wang, G. F. Wang, J. Wang, W. S. Wang, Y. S. Wang, X. Y. Wen, B. B. Wu, B. Y. Wu, M. Wu, G. C. Xiao, S. Xiao, S. L. Xiong, Y. P. Xu, Y. J. Yang, J. W. Yang, S. Yang, Y. J. Yang, Q. B. Yi, Q. Q. Yin, Y. You, A. M. Zhang, C. M. Zhang, F. Zhang, H. M. Zhang, J. Zhang, T. Zhang, W. Zhang, W. C. Zhang, W. Z. Zhang, Y. Zhang, Y. Zhang, Y. F. Zhang, Y. J. Zhang, Z. Zhang, Z. L. Zhang, H. S. Zhao, X. F. Zhao, S. J. Zheng, D. K. Zhou, J. F. Zhou, Y. Zhu, and Y. X. Zhu. Timing analysis of 2S 1417-624 observed with NICER and Insight-HXMT. , 491(2):1851–1856, Jan. 2020.

[24] A. S. Keith Arnaud, Randall Smith. *Handbook of X-ray Astronomy*, chapter 5.5.2. Cambridge Observing Handbooks for Research Astronomers. Cambridge University Press, 2011.

[25] R. L. Kelley, K. M. V. Apparao, R. E. Doxsey, J. G. Jernigan, S. Naranan, and S. Rappaport. Discovery of X-ray pulsations from 2S 1417-624. , 243:251–256, Jan. 1981.

[26] M. S. Longair. *High Energy Astrophysics*, chapter 13.1.3. Cambridge University Press, 3 edition, 2011.

[27] M. S. Longair. *High Energy Astrophysics*, chapter 13.4. Cambridge University Press, 3 edition, 2011.

[28] M. S. Longair. *High Energy Astrophysics*, chapter 13.5. Cambridge University Press, 3 edition, 2011.

[29] M. S. Longair. *High Energy Astrophysics*, chapter 19.6.1. Cambridge University Press, 3 edition, 2011.

[30] M. S. Longair. *High Energy Astrophysics*, chapter 14.6. Cambridge University Press, 3 edition, 2011.

[31] M. S. Longair. *The role of magnetic fields*, page 469–474. Cambridge Univ. Press, 2011.

[32] M. Nakajima, H. Negoro, M. Serino, T. Mihara, S. Ueno, H. Tomida, M. Ishikawa, Y. Sugawara, N. Isobe, R. Shimomukai, M. Sugizaki, S. Nakahira, W. Iwakiri, F. Yatabe, Y. Takao, M. Matsuoka, N. Kawai, S. Sugita, T. Yoshii, Y. Tachibana, S. Harita, Y. Muraki, K. Morita, A. Yoshida, T. Sakamoto, Y. Kawakubo, Y. Kitaoka, T. Hashimoto, H. Tsunemi, T. Yoneyama, T. Kawase, A. Sakamaki, Y. Maruyama, Y. Ueda, T. Hori, A. Tanimoto, S. Oda, T. Morita, S. Yamada, Y. Tsuboi, Y. Nakamura, R. Sasaki, H. Kawai, T. Sato, M. Yamauchi, C. Hanyu, K. Hidaka, T. Kawamuro, K. Yamaoka, and M. Shidatsu. MAXI/GSC detection of the outburst onset from the Be/X-ray binary pulsar 2S 1417-624. *The Astronomer's Telegram*, 11479:1, Mar. 2018.

[33] NICER-TEAM. Nicer data analysis threads - standard pipeline processing of an observation with "nicerl2".

[34] N. I. of Standards and T. of The United States. Fundemental physical constants: Newtonian constant of gravitation.

[35] M. Orellana and G. E. Romero. Gamma-Ray Emission from Be/X-ray Binaries. *Astrophys. Space Sci.*, 297(1-4):167–178, 2005.

[36] K. Pearson. On the criterion that a given system of deviations from the probable in the case of a correlated system of variables is such that it can be reasonably supposed to have arisen from random sampling. *Philosophical Magazine*, 50(5):157–175, 1900.

[37] R. A. Remillard, M. Loewenstein, J. F. Steiner, G. Y. Prigozhin, B. LaMarr, T. Enoto, K. C. Gendreau, Z. Arzoumanian, C. Markwardt, A. Basak, A. L. Stevens, P. S. Ray, D. Altamirano, and D. J. K. Buisson. An empirical background model for the NICER x-ray timing instrument. *The Astronomical Journal*, 163(3):130, feb 2022.

[38] M. M. Serim, Ö. C. Özüdoğru, Ç. K. Dönmez, Ş. Şahiner, D. Serim, A. Baykal, and S. Ç. İnam. Timing and spectral analysis of 2S 1417-624 during its 2018 outburst. , 510(1):1438–1449, Feb. 2022.

[39] S. A. Teukolsky.

[40] M. van der Klis. *Fourier Techniques in X-Ray Timing*, pages 27–69. Springer Netherlands, Dordrecht, 1989.

[41] M. van der Klis. Fourier techniques in x-ray timing. *2nd School on Multiwavelength Astronomy*, Jun 2010.